ENDOTHELIAL TIP-STALK CELL PATTERN FORMATION AS A FUNCTION OF GENE REGULATORY ARCHITECTURE

A Thesis

Presented to the Faculty of the Graduate School

of Cornell University

In Partial Fulfillment of the Requirements for the Degree of

Master of Science

by

William Robert Bedell

August 2014

ABSTRACT

Endothelial tip-stalk selection may determine the initial spacing of angiogenic sprouts from a previously uniform layers of cells. The mathematical model presented here predicts the onset conditions and equilibrium spacing of tip-stalk patterns in the presence of elevated VEGF. A linear stability analysis identified the network elements that enabled tissue-scale patterning, while a numerical simulation predicted the final density of tip cells. The assumptions of this model may have selected endothelial tip cells in an unusually high density if they were to become candidates for sprout outgrowth. Including filopodia or cytonemes that extended the effective range of juxtacrine signaling was only mechanism that enabled sparser patterns. This model provides an early experimental target for observing the controlled breakdown of symmetry in a uniform layer of mammalian cells as predicted by Turing, and may yield insight into the self-assembly of blood vessels, *in vitro* and *in vivo*.

BIOGRAPHICAL SKETCH

William (Bill) Bedell was born and raised in Portland, Oregon in the year 1991. He finished high school at Portland Community College in 2009 and graduated with honors from Oregon State University in 2012, earning a Bachelor of Science in chemical engineering. Bill loves chemical engineering for its combination of physics, math, biology, and educated guesses; it's the only thing as unfocused as him.

To my family, who made me;

and to my professors, who made me get to work.

ACKNOWLEDGMENTS

I would like to thank my advisor, Abraham Duncan Stroock, for his faith in my abilities since I first considered becoming a scientist. I extend my gratitude to my committee members, Jeff Varner and Julius Lucks; they will surely guide my path in the years to come. I owe much to my labmates, John Morgan , Mengrou Shan, and Lina Aboulmouna, whom I depend on daily. To my wonderful friends in Ithaca and beyond, I wish you all the same love and happiness you have given me.

TABLE OF CONTENTS

LIST OF FIGURES

CHAPTER 1

INTRODUCTION

Angiogenesis is the process by which the body expands the vasculature to supply nutrients to the tissues and achieve organism-wide homeostasis and immune function. In the adult, angiogenesis is associated with pathological conditions where it can be beneficial, as when it speeds the revascularization of wounds and tissue grafts; or harmful, as when tumors use the process to gain access to nutrients and metastasize. Though adult angiogenesis has been the target of recombinant protein therapy [1] and tissue engineering efforts [2], we still have an incomplete picture of the precise regulatory mechanisms that determine the quantitative (e.g. necessary morphogen concentration) and qualitative (e.g. vessel morphology) aspects of vascular growth. The mechanism that determines the initial site of an angiogenic sprout (Fig. 1 *A ii*) is an early and important target for the experimental and mathematical dissection of vascular morphogenesis, as it may shape the long-term evolution of a growing vasculature [3].

During angiogenesis, previously quiescent and homogeneous endothelial cells (Fig. 1 *A i*) differentiate into tip (t) and stalk (s) endothelial cells (Fig. 1 *A ii*) in response to hypoxic signals from nearby tissues, such as vascular endothelial growth factor (VEGF). Tip cells migrate towards the source of distress signals from oxygen-deficient tissues while stalk cells maintain the stability of the sprout and proliferate. These two sub-phenotypes of endothelial cell have been observed in the growing vascular plexus of the mouse retina [4], but it remains an open question whether planar

layers of endothelial cells (like those found in an adult vessel or a cultured monolayer) use tip-stalk selection to determine where sprouts will initiate.

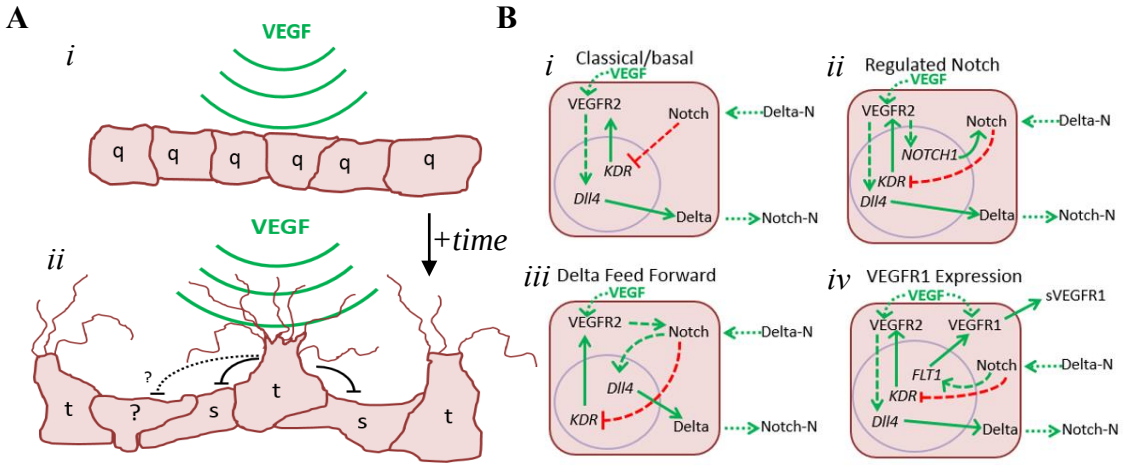

FIGURE 1 (*A*) Extracellular vascular endothelial growth factor (VEGF) induces a quiescent (*q*) endothelium (*i*) to pattern into the tip (*t*) and stalk (s) phenotypes (*ii*) [4]. The nascent tip cells extend filopodia and induce the stalk phenotype in neighboring cells to prevent them from responding to VEGF. Lateral inhibition of the tip phenotype is achieved through juxtacrine signaling between Delta ligand and Notch receptor [5], but there is uncertainty around the distance over which juxtacrine signaling can exchange information [6]. (*B*) The receptor Notch (*NOTCH1*), its ligand Delta (*DLL4*), and VEGF receptor 2 (*KDR*) form the classical basis of tip-stalk differentiation, but multiple hypothetical gene regulatory networks (GRNs) governing the mechanism have been proposed since its inception [7]. Dotted lines represent signaling, dashed line represent promotion (green) and repression (red), and solid lines represent protein expression.

Computational models exist [8, 9] that simulate tip-stalk selection based on empirical models of gene regulation [5, 10], but there is uncertainty about how the intracellular gene regulatory networks (GRNs; Fig. 1 *B*) and cell signaling network topology (Fig. 1 *A ii*) interact to achieve robust control over vessel stability and sprout density. Dysregulation of tip-stalk selection may be partially responsible the structural abnormalities of tumor vasculature, which has a tortuosity and stunted appearance consistent with an aberrantly high frequency of sprouting [11, 12].

This study formalizes some existing hypotheses [7] for the gene regulatory interactions underlying tip-stalk differentiation and develops experimentally testable predictions from their hypothetical kinetic rate laws. We couple a linear stability analysis to a numerical simulation of an endothelial cell network containing the GRNs shown in Figure 1 *B* to elucidate (1) the effective parameters that enable heterogeneous differentiation of neighboring cells in response to elevated VEGF and (2) the topological features of the gene regulatory network that determine spatial tip/stalk patterns.

CHAPTER 2

TIP-STALK PATTERN FORMATION BY DELTA-NOTCH

Angiogenesis: a branching phenomenon

Angiogenesis is a branching process, whereby an initial plexus (a primitive network of endothelial cells) extends, in a treelike pattern, sprouts that fuse to form an interconnected network of blood-filled endothelial lumens [13]. Previous work of developmental biologists [14] broke a similar process, that of tracheal morphogenesis in *Drosophila*, down into fundamental genetic programs; the first is *domain branching*, in which a layer of cells develops a spatially periodic pattern of differentiation. Those cells selected as the "peak" of the periodic pattern migrate away from the original surface (tip cells), thus creating (roughly) evenly spaced sprouts which elongate in the same direction. The classification of tip and stalk endothelial cells during sprouting angiogenesis (Fig. 1 *A ii*) emerged relatively recently from studies on the developing vasculature of the mouse retina [4].

Tip-stalk selection by lateral inhibition

The initial studies of endothelial tip-stalk selection confirmed VEGF as the signal that initiated this domain branching program from an otherwise quiescent endothelium [4], which was consistent with the established role of VEGF as an initiator of angiogenesis [15]. The highly conserved Notch signaling pathway was later found to enable the heterogeneous differentiation of tip and stalk cells [5], mirroring previous discoveries

that Notch controls branching morphogenesis in both tracheal and neuronal development by the process of lateral inhibition [16].

Lateral inhibition during tip-stalk differentiation works as follows: (1) An endothelial cell expresses on its surface a receptor tyrosine kinase (RTK) called VEGF receptor 2 (VEGFR2), which transduces the VEGF signal by trans-autophosphorylating (forming a phosphorylated VEGFR2 dimer) and activating numerous downstream pathways [17]. (2) Following VEGFR2 signal transduction, an endothelial cell will attempt to adopt a tip phenotype that is characterized by the increased expression of several genes and the extension of filopodia [18]. (3) A surface-bound ligand, Delta-like ligand 4 (DLL4/Delta) is expressed in nascent tip cells [19], and it activates Notch in neighboring endothelial cells (Fig. 1 *A*); Notch activation results in the cleavage of the Notch intracellular domain (NICD), which reduces the expression of VEGFR2 [1, 21] and prevents a Notch-activated cell from responding to VEGF.

Using Delta-Notch signaling, successful tip cells laterally inhibit their neighbors from responding to VEGF (Fig. 1 *A ii*) and relegate them to the stalk of a new sprout. In a plane of cells, this would produce a spatial pattern of tip cells (highly expressing Delta, VEGFR2, and filopodia) surrounded by stalk cells (with reduced expression of Delta, VEGFR2, and filopodia).

Hypothetical gene regulatory networks

A VEGFR2-Delta-Notch model alone (Fig. 1 *B i*; we shall refer to this as the "classical" mechanism for tip-stalk selection) is theoretically sufficient to produce a periodic pattern of tip and stalk cells if it follows previous mathematical treatments of lateral inhibition based on Hill-type functions of gene regulation [22]. However, numerous groups have suggested additional regulatory pathways that may influence the selection of tip and stalk cells and provide targets for experimentation. A review paper by Blanco and Gerhardt [7] summarizes the current scope of our understanding about the species and pathways implicated in tip- stalk selection, but in this paper we focus on three significant hypotheses inspired by experimental results over the last decade (Fig. 1 *B*).

Regulated Notch

An early work of Liu, *et al*. [10] suggested that the Notch receptor (as well as Delta) is up-regulated in certain types of endothelial cell when treated with VEGF (Fig. 1 *B ii*).

Delta Feed-Forward

A recent study by Caolo, *et al*. [23] suggested that the promotion of Delta by VEGFR2 signaling (Eq. 2) can only occur in the presence of Notch signaling (Fig. 1 *B iii*).The authors explain the crosstalk by pointing out that VEGFR2 signaling upregulates ADAM-17, a component of the Notch signaling pathway. VEGFR2 signaling therefore only interacts with the Notch-Delta signaling pathway by increasing the effective rate of Notch activation.

VEGFR1 Expression

Notch activation is known to increase the expression of VEGF Receptor 1 (FLT1), a receptor that inhibits the tip phenotype during angiogenesis [19] (Fig. 1 *B iv*). VEGFR1 is primarily thought to act as a "decoy" that prevents local VEGF from reaching VEGFR2 to induce the tip phenotype [25]. The discovery of a soluble form of VEGFR1 suggests the possibility of sVEGFR1 (*solube*-VEGFR1) modifying local VEGF profiles during tip-stalk selection using diffusion [26]

The complex crosstalk of these numerous signaling pathways and the uncertainty over precisely how they connect [24] motivates using theory to qualify the role each proposed mechanism would play in regulating the differentiation of tip and stalk cells.

Previous computational modeling of tip-stalk selection

An early and influential computational study by Bentley, *et al*. [8] used the "classical" network (Fig. 1 *B i*) in a cellular automaton simulation to reproduce tip-stalk selection in a linear array of cells. The simulation treated cells as hierarchical machines (cells were made up of many compartmentalized 'agents') with programmed rules that determined cell behavior (e.g. reduce # of VEGFR2 receptors) based on probabilistic functions of each agent's state (e.g. # of Dll4/Notch complexes). Model-specific parameters were chosen such that the global system displayed behavior congruent with *in vivo* micrographs during full simulations. The model expanded to recapitulate other phenomena, such as cell deformation in response to VEGF [27] and differential

adhesion during tip-stalk selection [28], by including more rules and complex behaviors into each agent of the simulation.

This computational model made powerful predictions that have guided experiments since its publication [25], but has some inherent limits of its applicability. The probabilistic and wholly discrete nature of the modeling approach limited mathematical analysis of the differential impacts of the assumed network topologies, kinetic rate laws, and parameter values of the regulatory networks underlying tip-stalk patterning. For example, the researchers could only investigate the interesting behavior of whole-system oscillation by sweeping various parameters over 50 runs instead of generating an analytical explanation for when and why oscillation occurred. The requirement of fine tuning model-specific parameters to achieve relevant global system behavior limits the potential of the agent-based modelling approach to extrapolate new phenomenon and aide in the design of experiments.

A parallel history of biological pattern formation

In contrast to the lineage of cellular automaton models that gave rise to Bentley's agent-based simulation, there is a history of using the principles of reaction kinetics and molecular transport to describe the formation of biological patterns. It began with Alan Turing's 1952 paper, "The Chemical Basis of Morphogenesis" [29]. This landmark work defined the general requirements needed by a system of interacting chemical reactions to produce spatial heterogeneity. Patterning was synonymous with a spatially homogeneous system becoming unstable, and Turing referred to this instability the "breakdown of symmetry". To determine if a system was capable of

breaking symmetry and forming a pattern, Turing simply performed a linear stability analysis about the homogeneous steady-state.

Biological pattern formation was later revisited by chemical engineers Hans Othmer and L.E. Scriven [30] with more convenient method for determining the stability of a cellular network. Individual cells were treated as separate compartments in an interconnecting lattice (Fig. 2). The connectivity or topology of this lattice was determined by the biophysical mechanisms that passed information between cells. In the case of juxtacrine Notch signaling, only cells which share a membrane border can exchange information in the Othmer-Scriven formulation.

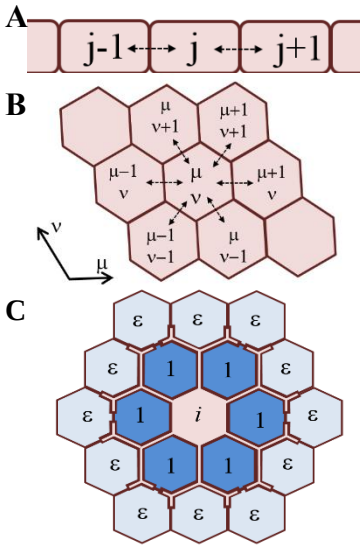

FIGURE 2 Graphical depiction of how a single cell communicates locally with its neighbors in two regular lattices, a one-dimensional "ring" (*A*) or a hexagonal lattice (*B*). Dotted lines show which cells exchange juxtacrine signals with the center cell, labeled as j or (μ, ν). Each cell in a ring has two neighbors, while a cell in a hexagonal lattice has six neighbors. (*C*) Filopodia may act as cytonemes or "tunnels" for Delta and Notch that extend the range of juxtacrine signaling to second-nearest neighbors. Immediate neighbors of the center cell (i) still have the strongest signaling interactions, and are weighted as order 1 when calculating neighboring Delta levels ($\langle D \rangle_i$, Eq. 22); cells only in contact with filopodia have a weight scaled down to a factor ε.

Real cell monolayers are never perfectly ordered, but the approximation of a regular lattices gives reasonable estimates for qualitative patterning from juxtacrine signaling by, for instance, allowing us to estimate what length in cell-diameter-equivalents there should be between tip cells. As we will discuss in the Methods section, "Extended Signaling Networks", this lattice model can also incorporate

longer-range interactions (Fig. 2 *C*) that may be facilitated by filopodia acting as cytonemes. This has been proposed to influence Delta-Notch pattern formation in *Drosophila* [6].

Years after Othmer & Scriven published their work, Collier *et al* [22] used new discoveries in the juxtacrine signaling of Delta and Notch to explore how lateral inhibition could amplify random perturbations of a homogeneous steady-state to produce "checkerboard" patterns of primary (tip cells in our model) and secondary (stalk) phenotypes. Plahte [31] incorporated the Othmer-Scriven method of linear stability analysis to the topic of patterning by juxtacrine signaling to simplify the process of determining stability in the Delta-Notch system. Plahte's study first established the requirement of high cooperativity in the gene regulatory interactions between species (approximated as Hill functions) for patterning to occur.

Following this mathematical history, Sprinzak, *et al*. [32] reignited the topic of Delta-Notch patterning with powerful experiments enabled by advances in synthetic biology. The approach of using ODEs to predict patterning results based on measurable parameters allowed the researchers to rule out and propose hypotheses about the signaling and gene regulatory networks underlying Delta and Notch patterning. This team measured, for instance, the cooperativity of a Notch downstream promoter and compared it to the theoretical requirement set forth by Plahte. Finding the measured cooperativity too low to produce patterning, the team predicted and found experimental evidence for a novel kinetic rate law for between Delta-like ligand

1 (DLL1) and Notch1 that could enable patterning in the absence of high cooperativity.

Adapting the Turing framework to endothelial patterning

Encouraged by this recent success in the modeling and testing of Delta-Notch gene regulation, we will apply the ODE-based mathematics of biological pattern formation to the specific context of endothelial tip-stalk differentiation. We will start by modeling the classical GRN first formalized by Bentley [8] using differential equations for the expression of VEGFR2 and Delta, and simple kinetic rate laws for the signaling of VEGFR2 and Notch. The scientific consensus is that the regulation of both Delta and VEGFR2 availability during tip-stalk differentiation occurs primarily at the transcriptional level (as opposed to allostery or degradation) [5, 20, 21, 23, 25, 33], so changes in gene expression will be accomplished by modulating protein generation rates.

All cellular processes between a signaling event and a corresponding output in protein production will be coarse-grained into repressive or activating Hill functions [34]. In essence, a Hill function is a generalization of our current linear understanding of gene regulation in this system (e.g. NICD down-regulates VEGFR2 expression). Likewise, a Boolean function is a Hill function where the Hill coefficient approaches infinity. The use of Hill functions permits us to quantify how close the complete regulatory interaction is to either linear (gradual) or Boolean (steep).

The use of explicit equations for modeling our GRNs permits us to use a linear stability analysis to develop a criteria for pattern formation in the tradition of Turing. Numerical simulation of the ODEs will be used to investigate the spatial results of patterning in multiple geometric lattices. All of the different GRN hypotheses of Figure 1 *B* will not be implemented simultaneously: each will be given a separate treatment so we can gain an intuitive understanding of their potential role in tip-stalk patterning. By coupling analytical and numerical formalism with holistic experimental design, we shall evaluate the pattern formation of tip and stalk cells as a viable theory for the initial gene regulation and sprouting density of angiogenesis in the adult vessel and *in vitro* endothelium.

CHAPTER 3

MODELS AND METHODS

The Turing-like model of tip-stalk selection

The gene regulatory network underlying "classical" tip-stalk selection (Fig. 1 *B i*) can be represented by differential equations for VEGFR2 (R_i) and Delta (D_i)

$$\frac{dR_i}{dt} = \beta_R \frac{(k_{RNA})^{n_R}}{(k_{RNA})^{n_R} + (N_{Ai})^{n_R}} - \gamma_R R_i \tag{1}$$

$$\frac{dD_i}{dt} = \beta_D \frac{(R_A)^{n_D}}{(k_{DRA})^{n_D} + (R_{Ai})^{n_D}} - \gamma_D D_i \tag{2}$$

Here, the subscript i refers to an individual cell in a lattice of N cells; each cell is governed by identical ODEs, but expression and signaling levels will differ when the tissue patterns, as we shall see. In Eqs. 1 and 2, R_i and D_i refer to the surface expression levels of VEGFR2 and Delta with units of *number/cell*, referring to the numbers of each protein available for signaling. Each species is produced by activating or repressing Hill function scaled by production rates β_R and β_D, with units *number/cell/hour*.

The Hill functions of Eqs. 1 and 2 use as inputs the signaling events for Notch (N_{Ai}) and VEGFR2 (R_{Ai}), also with units *number/cell*, respectively referring to the level of NICD and phosphorylated VEGFR2 monomer. Each Hill function is governed by two parameters: the dissociation constants (k_{RNA} and k_{DRA}), which establish the 'threshold' signaling activities that result in gene expression at ½ max; and the Hill

coefficients (n_R and n_R), which model the effective cooperativity of each regulatory interaction and determine the steepness of the Hill function. The production rates of each species are balanced by first-order decay rates γ_R and γ_D, which are assumed to be static in this model and incorporate the average rate of degradation, the dilution of protein concentration due to cell division, or both.

The formation of a phosphorylated VEGFR2 monomer (R_{Ai}) is modeled as the reversible formation of a VEGF-VEGFR2 complex:

$$\frac{dR_{Ai}}{dt} = k_{V+}V_i(R_i - R_{Ai}) - k_{V-}R_{Ai} \tag{3}$$

where V_i refers to the local concentration of vascular endothelial growth factor (VEGF) available to the VEGFR2 receptors (measured in pM), k_{V+} is the rate of the forward reaction, and k_{V-} is the rate of the reverse reaction. Because the dynamics this association are very fast (Order seconds [35]) compared to the time scales of gene expression (Order hours-days, [10]), we can approximate R_{Ai} as pseudo-steady-state:

$$R_{Ai} = \frac{V_i R_i}{\frac{k_{V-}}{k_{V+}} + V_i} \tag{4}$$

where $\frac{k_{V-}}{k_{V+}}$ can be redefined as binding affinity (K_V) for VEGFR2 and VEGF, which has been measured to be 600-800 pM [36, 37]. Provided that VEGF is present levels well below this concentration, such as those observed in cancer samples (1 – 300 pM [38]), we can further simplify the expression for VEGFR2 activation to a simple product:

$$R_{Ai} = \frac{V_i R_i}{K_V} \tag{5}$$

The reality of the VEGFR2-VEGF reaction is far more complex, as we shall briefly consider in a later section, "Nonlinear Signaling Kinetics."

Changes in gene regulation downstream of Notch are accomplished by NICD after the transactivation of Notch by neighboring Delta. The level of NICD in cell i is given by the equation,

$$\frac{dN_{Ai}}{dt} = \frac{N_i}{\nu k_N} \sum D_{j \neq i} - \gamma_{NA} N_{Ai} \tag{6}$$

NICD is generated by a first order reaction between local Notch (N_i) and the average concentration Delta in neighboring cells ($D_{j \neq i}$), and it is depleted by first-order decay rate (γ_{NA}). Here, ν is the number of neighboring cells in contact with cell i. In this equation, the number of available Notch receptors per cell (N_i) is assumed to be constant. The decay of NICD is coordinated by multiple species, but with a half-life of ~180 min [38], we consider the response time to be faster than the changes in gene expression.

Like VEGFR2 signaling, we shall approximate the level of NICD as pseudo-steady-state,

$$N_A = \frac{N_i}{\nu k_N \gamma_{NA}} \sum D_{j \neq i} \tag{7}$$

The juxtacrine signaling network of Delta-Notch

The production of NICD (Eq. 7), which takes as an input the average Delta expression of neighboring cells ($D_{j\neq i}$), defines the structure of cell signaling network (Fig. 2) by limiting the exchange of information to the nearest neighbors in a regular lattice of cells. We can potentially improve the realism of this model by incorporating the proposed action of filopodia as long-distance tunnels for Notch signaling; this will be discussed in a later section, "Extended Signaling Networks".

At the capillary scale, the endothelium is reticulated network of semi-linearly-arranged cells (Fig. 2 *A*), with multiple cells between a branching points (the exact number of "edge" cells is an open question). Locally, the cells might be modeled as a string of cells (Fig. 2 *A*), as they were in [8].

Conversely, mature blood vessels are a topologically two-dimensional surface (Fig. 2 *B*) (assuming cells only exchange juxtacrine signals with neighbors in their local plane) mapped onto a 3D cylinder. A periodic boundary condition (PBC) can be employed for the moderately-sized circumference of the vessel, while a long (many-celled) domain with a PBC can approximate the axial length of the vessel.

In vitro angiogenesis assays of endothelial cells initially start with a two dimensional geometry in the form of a cultured monolayer [40, 41], so a hexagonal lattice (Fig. 2 z) with a large grid size is quite appropriate.

Nondimensionalization

Equations 1 and 2 of the classical GRN can be redefined in terms of a limited number of dimensionless parameters,

$$\frac{d\mathcal{R}_i}{d\tilde{t}} = \frac{(\kappa_R)^{n_R}}{(\kappa_R)^{n_R} + (\langle\mathcal{D}\rangle_i)^{n_R}} - \mathcal{R}_i \tag{8}$$

$$\frac{d\mathcal{D}_i}{d\tilde{t}} = \frac{(\mathcal{V}_i\mathcal{R}_i)^{n_D}}{(\kappa_D)^{n_D} + (\mathcal{V}_i\mathcal{R}_i)^{n_D}} - \tau\mathcal{D}_i \tag{9}$$

where $\mathcal{R}_i = \frac{\gamma_R}{\beta_R}R_i$, $\mathcal{D}_i = \frac{\gamma_D}{\beta_D}D_i$, $\mathcal{V}_i = \frac{V_i}{K_V}$, $\tau = \gamma_D/\gamma_R$, and $\tilde{t} = t\gamma_R$. Most of the parameters have been lumped into two effective dissociation constants

$$\kappa_R = \frac{k_{RNA}\gamma_D}{\tau\mathcal{N}_i\beta_D} \tag{10}$$

$$\kappa_D = \frac{k_{DRA}\gamma_R}{\beta_R} \tag{11}$$

where $\mathcal{N}_i = \frac{N_i}{k_N\gamma_{NA}}$. This formulation is convenient because both $\mathcal{R}_i$ and $\mathcal{D}_i$ range from 0 to 1 when $\tau = 1$ (corresponding to roughly equal rates of response in gene expression), leaving the system behavior to be wholly determined by κ_R, κ_D, $\mathcal{V}_i$, n_R, and n_D.

Linear stability analysis

A quiescent (non-sprouting) endothelium can be said to be stable at the homogeneous steady-state (HSS) of differentiation because it remains homogeneous when subjected to minor fluctuations in gene expression or signaling activity. Conversely, it can be

said that a network of endothelial cells which spontaneously patterns into tip and stalk phenotypes is unstable at the homogeneous steady-state. By assuming that the initial condition of a network of endothelial cells is homogeneous, we can perform a linear stability analysis around the HSS of differentiation to determine the criteria for an endothelium to break symmetry and pattern into tip and stalk cells based on our choice of kinetic rate laws. See Appendix A1 for a more detailed derivation of this analysis.

We start by performing first-order expansion of Eqs. 1 and 2 about the point where Delta (D_{ss}) and VEGFR2 (R_{ss}) expression is steady and equivalent in every cell of our lattice. The partial derivatives of each species (n species) in each cell (N cells) is arranged into a vector-of-vectors $\boldsymbol{X}$ that allows us to write our system of n x N differential equations in terms of one larger equation,

$$\frac{d\boldsymbol{X}}{dt} = (\boldsymbol{I_N}\otimes\boldsymbol{K} + \boldsymbol{M}\otimes\boldsymbol{B})\boldsymbol{X} = \boldsymbol{J}\boldsymbol{X} \tag{12}$$

$\boldsymbol{K}$ and $\boldsymbol{B}$ are $n \times n$ matrices (2×2 for the classical GRN) that contain the linearized forms of each differential equation, and $\boldsymbol{M}$ is an $N \times N$ 'connectivity matrix' that formalizes the structure of our signaling network, like in Fig. 3 below. $\boldsymbol{K}$ accounts for cell-autonomous processes are independent of neighboring cells (e.g. $\frac{d\dot{D}_i}{dR_i}\Big|_{ss}$). $\boldsymbol{B}$ accounts for signaling-dependent processes that depend on the chemical content of

neighboring cells (e.g. $\frac{d\dot{R}_i}{d\langle D\rangle_i}\Big|_{ss}$). Full examples of the matrices $\boldsymbol{K}$ and $\boldsymbol{B}$ for each GRN can be found in Appendices A2-A5.

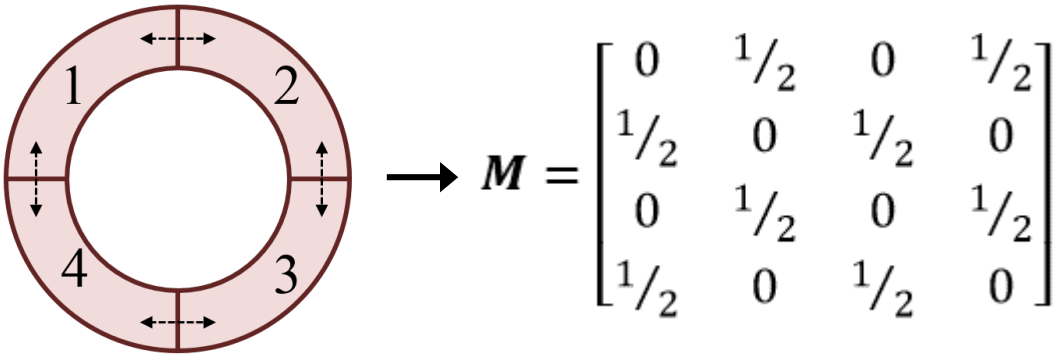

FIGURE 3 Translation of a 1-dimensional string with a periodic boundary condition into a connectivity matrix. The eigenvalue of **M** is called the structural eigenvalue (q_k), and it is used in the final stability criteria.

The eigenvalues of our Jacobian $\boldsymbol{J}$ (Eq. 12) determine the local *Maximal Lyapunov Exponent* (MLE) at the homogeneous steady-state; a positive MLE corresponds to an unstable endothelium that will pattern into tip and stalk cells. We can transform our Jacobian to be in the orthonormal basis of our connectivity matrix; this means for a given "structural eigenvalue" (q_k) of our connectivity matrix, we only have to find two MLE eigenvalues instead of $2N$ eigenvalues.

The MLE eigenvalues ($\lambda_{k\mu}$) are found using the equation,

$$\det\left(\boldsymbol{K} + q_k\boldsymbol{B} - \lambda_{k\mu}\boldsymbol{I_n}\right) = 0 \tag{13}$$

Using the classical GRN (Fig. 1 *B i*), the condition that results in a positive MLE eigenvalue is

$$-q_k \frac{\partial \dot{R}_i}{\partial \langle D_i \rangle}\bigg|_{SS} \frac{\partial \dot{D}_i}{\partial R_i}\bigg|_{SS} - \frac{\partial \dot{R}_i}{\partial R_i}\bigg| \frac{\partial \dot{D}_i}{\partial D_i}\bigg| > 0 \tag{14}$$

The left hand side of this inequality is proportional and equal in sign to the local MLE at the homogenous steady-state and will be referred to as the "MLE" in later sections.

Numerical modeling

Simulation of the endothelial patterning was carried out in MATLAB using the ode45 numerical integrator and the dimensionless Eqs. 8 and 9. The Hill coefficients n_R and n_D were set to 2 to supply the necessary degree of cooperativity (as dictated by the analytical stability criteria, see Results), while the concentration of VEGF was varied over the physiological range measured in angiogenic tumor samples, 1 – 300 pM [38]. The ratio of VEGFR2 and Delta decay constants, τ, was set to 1 under the assumption that both species decay at roughly the same rate. Appropriate parameters κ_R and κ_D from Eqs.10 and 11 were first determined using the analytical stability criteria (see Figure 6).

The program executed by calculating the homogeneous steady state (HSS) values for $\mathcal{R}$ and $\mathcal{D}$, and then integrating the two ODEs for each cell in the lattice after subjecting the lattice to a minor ($\ll 1\%$) random perturbation in Delta expression at the initial condition. The integration proceeded until the system reached a new steady state.

Extension to other hypothesized GRNs

The mathematical framework we have used to model classical tip-stalk patterning can be extended to other hypothesized GRNs (Fig. 1 *B*) by altering our system of differential equations. The methods we use to analyze the equations are the same, and we can generate linear stability criteria for each case using the same method of linear stability analysis (Eqs. 12 and 13). We shall now establish the mathematical treatment we will give each hypothetical variation of the GRN.

Basal expression

This variation (Fig. 1 *B i*) covers the expectation that neither species (Delta or VEGFR2) will be completely depleted at the limit of signaling (Low VEGF, high neighboring Delta). It is modeled by including constant additive terms in the differential equations for gene expression

$$\frac{dR_i}{dt} = \alpha_R + \beta_R \frac{(k_{RNA})^{n_R}}{(k_{RNA})^{n_R} + (N_A)^{n_R}} - \gamma_R R_i \tag{15}$$

$$\frac{dD_i}{dt} = \alpha_D + \beta_D \frac{(R_A)^{n_D}}{(k_{DRA})^{n_D} + (R_A)^{n_D}} - \gamma_D D_i \tag{16}$$

Regulated Notch receptor

We can model the regulation of Notch by VEGF-VEGFR2 (Fig. 1 *B ii*) by adding a third ODE which governs Notch expression in response to VEGFR2 signaling

$$\frac{dN_i}{dt} = \beta_N \frac{(R_A)^{n_N}}{(k_{NRA})^{n_N} + (R_A)^{n_N}} - \gamma_N N_i \quad (17)$$

The parameters used here follow the same nomenclature as Eqs. 1 and 2.

Delta Feed-Forward

Under the "Delta Feed-Forward" GRN (Fig. 1 *B iii*), Notch regulation directly upregulates Delta expression and downregulates VEGFR2 expression. The ODE for Delta expression is therefor given by

$$\frac{dD_i}{dt} = \beta_D \frac{(N_A)^{n_D}}{(k_{DNA})^{n_D} + (N_A)^{n_D}} - \gamma_D D_i \quad (18)$$

In line with the predictions by Caolo, et al [23] that VEGFR2 signaling modulates Notch signaling through the ADAM-17 metalloprotease, we incorporate an activating Hill function of VEGFR2 activation in the kinetic rate law for Notch activation

$$N_{Ai} = \frac{N_i}{nk_N\gamma_{NA}} \sum D_{j\neq i} \left(\frac{(R_{Ai})^{n_A}}{(k_{NRA})^{n_A} + (R_{Ai})^{n_A}} \right) \quad (19)$$

The intermediate reactions that facilitate this interaction might be more accurately treated with a third ODE, but we ignore this possibility for the time being to establish a limiting case where the action of VEGFR2 on Notch signaling is fast compared to changes in gene expression.

VEGRFR1 expression

VEGFR1, which is up-regulated by Notch signaling (Fig. 1 *B iv*) and reduces VEGFR2 signaling in endothelial cells, is present in soluble (sVEGFR1) and membrane-bound isoforms (mVEGFR1). We can model the expression and diffusion of (s/m)VEGFR1 by using our typical kinetic expression (e.g. Eq 1) with an added term that approximates Fickian diffusion.

$$\frac{dS_i}{dt} = \beta_S \frac{(N_A)^{nS}}{(k_{SNA})^{nS} + (N_A)^{nS}} - \gamma_S S_i + \frac{K_s}{\nu} \sum \left(S_{j \neq i} - S_i\right) \tag{20}$$

where S_i in this expression refers to the effective availability of VEGFR1 in the compartment of cell i; we do not discriminate between sVEGFR1 and mVEGFR1. In Eq. 20, we use a discretized analog of the Fickian equation with diffusion coefficient K_s that ignores flux into the bulk of the fluid surrounding the endothelium. This flux can be effectively included in the first-order decay rate γ_S if we assume that sVEGFR1 is dilute outside the immediate influence of the endothelium.

We model the VEGFR2-inhibiting properties of VEGFR1 by modifying Eq. 5 to scale the down the number of VEGF-VEGFR2 complexes.

$$R_A = f(V_i, R_i, S_i) = \frac{V_i R_i}{k_v(1 + k_s S_i)} \tag{21}$$

Here, k_s is the parameter that controls the strength of VEGF-VEGFR2 inhibition by VEGFR1. There is disagreement in the literature about whether VEGFR1 reduces VEGFR2 signaling by sequestering extracellular VEGF or by forming nonproductive heterodimers with VEGFR2 [42, 43], but this approximation is agnostic about the distinction.

Other system consideration

Extended signaling networks

Though the juxtacrine signaling of Delta and Notch is usually assumed to only occur between adjacent cells that share a significant membrane border [22], we wanted to investigate what would happen if the range of juxtacrine signaling was extended beyond the nearest neighbors in a regular lattice. A recent study [6] in the Delta-Notch patterning of the Drosophila embryo proposed that filopodial extensions from nascent "bristle" (analogous to tip) cells act as cytonemes, or signaling "tunnels", that laterally inhibited distant (≥ 2 cells away) neighbors by distributing Delta ligands

We can mirror this hypothesis by including second-nearest neighbors in the calculation of the average Delta expressed in neighboring cells. Here, second-nearest neighbors are weighted lower in determining neighboring Delta concentrations by a factor ε.

$$N_A = \frac{N_i}{(\nu_{1^\circ} + \varepsilon\nu_{2^\circ})}\left(\sum D_{1^\circ} + \sum \varepsilon D_{2^\circ}\right) \tag{22}$$

Where 1° refers to nearest neighbors and 2° refers to second-nearest neighbors.

Nonlinear signaling kinetics

In Eq. 5, we model the activation of VEGFR2 as a product of the receptor and ligand (VEGF) concentrations. In reality, the kinetics of VEGFR2 activation are considerably

more complex than the enzyme kinetics Michaelis-Menten are modeled upon. VEGFR2 is translated as a monomer, but must dimerize before it can phosphorylate, so there may be some nonlinear action between VEGFR2 monomers to ultimately produce phosphorylated complexes. This may manifest as an apparent exponent on the expression level of VEGFR2 in the equation for VEGFR2 activation:

$$R_A \sim \frac{V_i {R_i}^{n_a}}{k_V} \tag{23}$$

Our estimation based on the computational work of MacGabhann [44] indicates the apparent exponent may be as high as 1.7.

CHAPTER 4

RESULTS

Instability is a natural trajectory away from uniformity

The selection of tip and stalk cells from an endothelium closely follows the problem of pattern formation as predicted by Turing [29], in which a network of cells with a uniform initial condition breaks symmetry based on the coupled signaling and regulation of her genes. Theory dictates that a multicellular pattern can only form out of a uniform initial condition (such as a newly deposited monolayer of endothelial cells) if the homogeneous steady-state (HSS) is unstable to perturbations. If the response of a perturbation decays towards the HSS as the cells iteratively process signals, the system is stable; if the perturbations grows with time, the system is unstable.

We can explain this by plotting the average amount of Delta a cell detects by Notch signaling versus the amount of Delta ligand she expresses at steady-state, as shown in Figure 4 for the classical GRN (Fig. 1 *B i*). Figure 4 is known as a cobweb plot, or iterative map, because it shows the steady-state a system would reach after every cycle of imposition and response [45]. In this way, we can visualize the time-course of the system and determine if it is stable or unstable.

A system that is stable decays back to the homogeneous steady state after an initial perturbation is imposed (Fig. 4 *A*), while an unstable system grows with every iteration (Fig. 4 *B*). Note that the unstable systems in these plots have slopes that are

< -1 at the homogeneous steady-state; this will be referenced in the linear stability criteria.

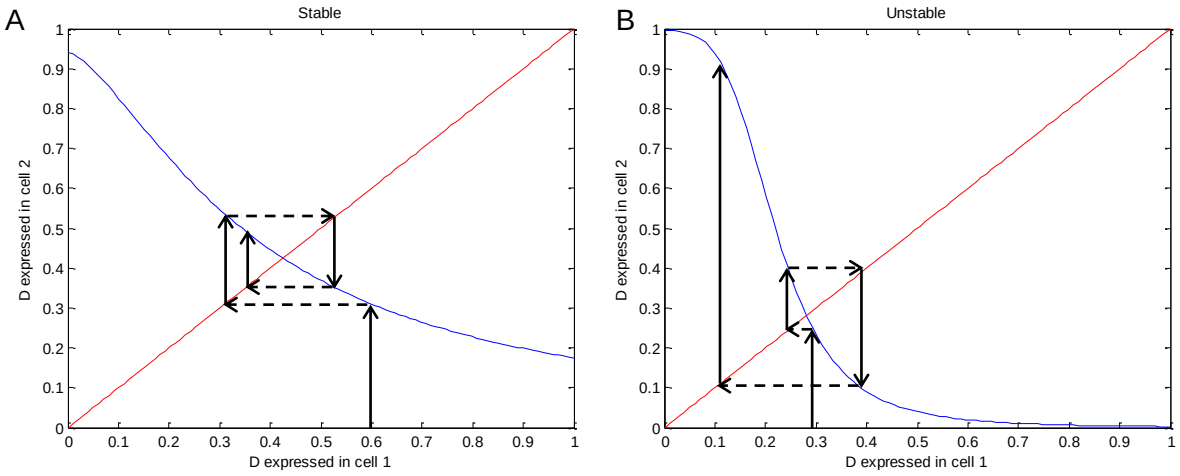

FIGURE 4 The pseudo-steady-state input and output of Delta expression in a two cell model. In the stable plot (*A*), the initial perturbation (D1 = 0.6) decays back towards the HSS. In the unstable case, the deviation from the HSS in the initial perturbation (D1 = 0.3) grows quickly. In this model, the solid black arrows show how each cell responds to its input, while the dashed arrows transfer the output from the previous iteration to the input. Parameters have been exaggerated for illustrative purposes.

Patterning requires multiple steady-states

Steady-states in this model correspond to non-transient cell phenotypes that have the potential to exist indefinitely, and they are found by setting our ODEs (Eqs. 1 and 2) to zero to specify the lack of change over time. A system that will pattern into tip and stalk cells will likely have multiple steady-states of Delta expression, representing (1) the unstable HSS, (2) a highly-expressing state corresponding to tip cells, and (3) a state with low Delta expression corresponding to stalk cells. Because each cell in our lattice communicates to neighboring cells and responds with changes in gene output, all possible steady-states are part of multicellular feedback loops; in a patterned lattice, tip cells are only at steady-state when surrounded by stalk cells. To find these states,

we can generate a plot that iterates the cycle of 'Delta imposed versus Delta expressed' twice. In a two cell model, this recursive function represents the Delta a cell will 'want' to express in response to its own expression level, and a real steady-state exists only where the inputs and outputs are equal.

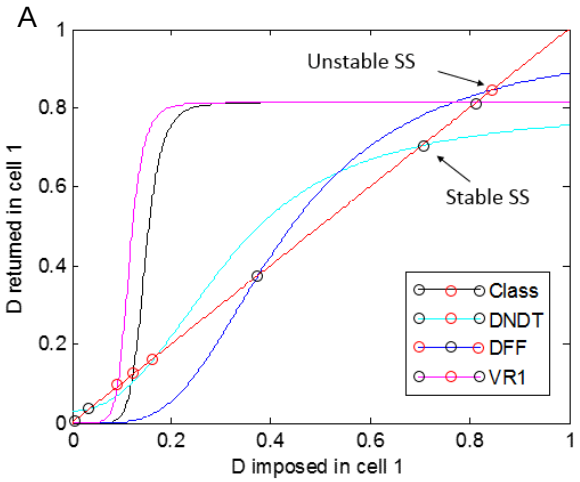

FIGURE 5 The steady-states of each GRN variation were found by imposing a Delta output in a cell and calculating the resulting Delta output after two pseudo-steady-state recursions in a two-cell model. An intersection with y = x is a possible steady-state. Regulated Notch (*DNDT*) made the patterned states closer to the homogeneous state, while VEGFR1 regulation (*VR1*) lowered the homogeneous steady-state concentration of Delta. Unlike the other GRNs, Delta Feed-Forward (*DFF*) had one stable HSS, and two unstable states of spatially homogeneous differentiation.

Figure 5 shows the steady-state inputs and outputs of each GRN over the range of nondimensional Delta expression. The differences between each variation of the GRN are close to trivial in this plot: each one is a monotonic sigmoid that intersects the $y = x$ line in three places, representing the three predicted steady-states (high/tip; medium/homogeneous; low/stalk). The nullcline of the "Delta Feed-Forward" GRN appears to be qualitatively the same as the other three, but in fact, it has only homogeneous steady-states and will never form a pattern. To explain these nullclines and their relation to patterning, we need to use a linear stability analysis.

The analytical stability criteria

We have identified that each GRN can potentially produce multiple steady-states, but we have not established whether the cells will remain in the steady-state phenotypes if subjected to minor perturbations. Linear stability analysis is a method of determining if a system is stable or unstable about a particular point using a first-order series expansion. The eigenvalues of that expansion determine whether a system is locally stable (if all eigenvalues are negative) or unstable (if some eigenvalues are positive). In dynamical systems, the most positive eigenvalue is referred to as the Maximal Lyapunov Exponent (MLE), and it is the fastest growing trajectory of the system after an initial perturbation.

By leaving the differential equations that govern our system in terms of generic parameters, we were able to derive analytical criteria for determining the stability of a HSS for each GRN. The criteria for instability from the classical case (Eq. 14) established the broad characteristics needed by endothelial cells to pattern into tip and stalk cells from a uniform initial condition using lateral inhibition (Table 1).

Under the classical case, the "-1" in the stability criterion is analogous to the requirement laid out in the cobweb plot (Fig. 4), that the derivative of the GRN must be lower than -1; this requirement represents the natural tendency of the system to decay back to its previous state. The term ($-q_k n_R n_D g_R g_D$) that overcomes the natural stability is a linearized representation of lateral inhibition. It consists of three parts: the structural eigenvalue (q_k), the effective Hill coefficients of gene regulation (n_R, n_D), and the functions g_R and g_D, defined by

TABLE 1 Criteria for instability for the various hypothesized GRNs

GRN Variations	Criteria for instability ($LHS \propto MLE$)	Ref.
Classical GRN	$-q_k n_R n_D g_R g_D - 1 \geq 0$	Hellstrom (2007)
Basal expression	$-q_k n_R n_D g_R g_D \left(1 - \frac{\alpha_R}{R_{ss}\gamma_R}\right)\left(1 - \frac{\alpha_D}{D_{ss}\gamma_D}\right) - 1 \geq 0$	Prediction
Regulated Notch receptor	$-q_k n_R n_D g_R g_D - \frac{\gamma_N}{\gamma_D} n_N n_R g_N g_R - 1 \geq 0$	Liu (2003)
Delta "Feed Forward"	$q_k g_D n_D - g_A g_R n_R n_A - 1 \geq 0$	Caolo (2010)
VEGFR1 expression	$-q_k n_R n_D g_R g_D - q_k \frac{n_D n_S g_D g_S}{\left(1 + (1 - q_k)\frac{K_S}{\gamma_S}\right)} \frac{k_s S_{ss}}{1 + k_s S_{ss}} - 1 \geq 0$	Suchting (2007)
Nonlinear signaling	$-q_k n_R n_D n_a g_R g_D - 1 \geq 0$	MacGabhann (2007)

$$g_R = \frac{(K_N D_{ss} N_i)^{n_R}}{(k_{RNA})^{n_R} + (K_N D_{ss} N_i)^{n_R}} \tag{24}$$

$$g_D = \frac{(k_{DRA})^{n_D}}{(k_{DRA})^{n_D} + \left(\frac{V R_{ss}}{k_V}\right)^{n_D}} \tag{25}$$

The functions g_R and g_D originate from the derivatives of the Hill functions governing gene expression and they are bounded by 0 and 1. Using the dimensionless Equations 8 and 9, these functions can alternatively be written as $g_R = 1 - \mathcal{R}_{ss}$ and $g_D = 1 - \mathcal{D}_{ss}$.

In the stability criteria of Table 1, q_k (there are *N* of them) are the 'structural eigenvalues' of the modes on which the system can pattern [30], and they are the eigenvalues of our connectivity matrix M (see Fig. 3). In this system the largest negative eigenvalue of M is the most unstable, because it makes the MLE the most positive. In a normal lattice (Fig. 2 *A* & *B*), the largest negative structural eigenvalue

corresponds to two immediately neighboring cells bifurcating in opposite directions, so a close-packed 'checkerboard' pattern is the fastest patterning mode of the network.

The largest negative eigenvalues in q_k range from -1 for a linear array of cells (Fig. 2 *A*) to -0.5 for a hexagonal array of cells (Fig. 2 *B*), and this determines the minimum magnitude the remaining terms ($n_R n_D g_R g_D$) must exceed for the MLE to become positive and the HSS to be unstable. The functions g_R and g_D have upper bounds of 1 (corresponding to very little steady-state expression of either species), so for a hexagonal lattice with a minimum structural eigenvalue of -0.5, the product of the exponents ($n_R n_D$) from each Hill function must exceed 2 for patterning to be possible; in practice, this product must well exceed 2 to account for the product of g_R and g_D being less than 1.

From this simple analysis, we can see that any lateral inhibition mechanism approximated by Hill functions needs a significant degree of nonlinearity in the gene regulatory functions to form a pattern.

Stability criteria of the GRN variations

We have established how an endothelium can become unstable and pattern based on the fundamental mechanism of lateral inhibition. The criterion for instability in the classical GRN contains the destabilizing influence of lateral inhibition, and this mathematical term ($-q_k n_R n_D g_R g_D$) is conserved in the stability criteria of the GRN variations because they include lateral inhibition feedback loop with additional

pathways. The analytical criteria for instability for each variation of the GRN is given in Table 1.

The criteria for the remaining hypothesized GRNs include differences in the MLE to reflect how the lateral inhibition mechanism is deteriorated ("Regulated Notch") or enhanced ("VEGFR1 expression") by the new kinetic rate laws. Note that in the case of "Nonlinear signaling", which only added nonlinear kinetics to the kinetic rate law for VEGFR2 signaling (Eq. 23), the difference is an additional term in the product of exponents ($n_R n_D n_a$). Based on these results, all of the effective Hill coefficients for gene expression (n_R, n_D, etc) were assumed to be 2 in the numerical portions of the study.

Instability and patterning are switched on or off by VEGF

The classical model of tip-stalk selection was intended to explain the observation that increased levels of VEGF facilitated endothelial patterning into tip and stalk phenotypes [8]. In mathematical terms, the spatially uniform state of differentiation in the endothelium should switch from stable to unstable when the uniform concentration of VEGF passes a certain value. Because our system is nonlinear, it is not possible to generate an explicit equation for the VEGF concentration (V_i) that switches the system from stable to unstable, so we used a numerical evaluation of the stability criterion to find this concentration.

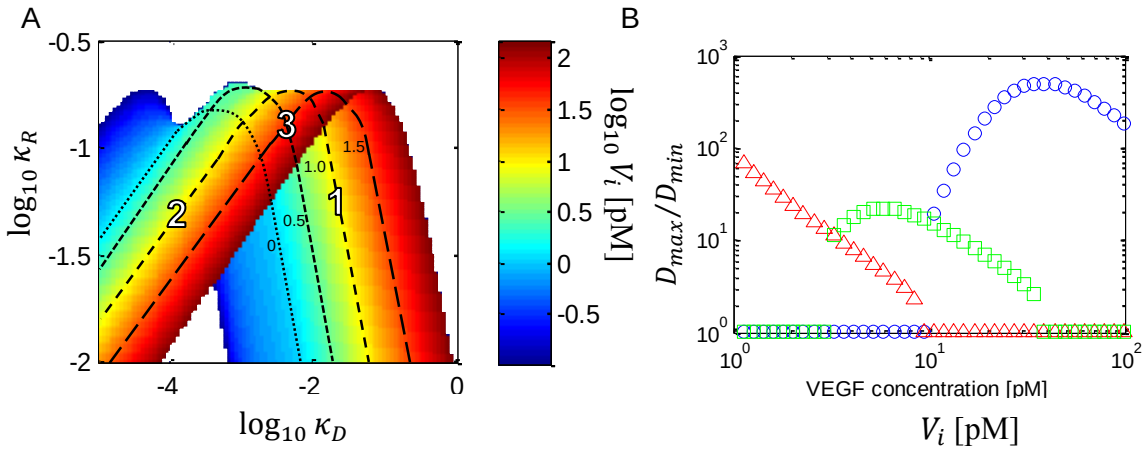

FIGURE 6 (*A*) A surface of critical stability (MLE = 0) for different combinations of dimensionless parameters κ_D and κ_R shows the switching behavior of the system at physiologically relevant levels of VEGF [1 pM (light blue) – 100 pM (red)]. Three regions arise from this constraint: region "1" in which the system is stable at low [VEGF] but becomes unstable at high [VEGF]; the unrealistic region "2" which is unstable at low [VEGF] but becomes stable at high [VEGF]; and the overlapped region "3" in which there is a window of instability with respect to [VEGF]. No critical VEGF concentrations were found in the physiological range for the white areas of the figure. (*B*) The simulated final steady states of Delta expression bifurcate over predictable ranges of VEGF conditions in regions 1 (circle), 2 (triangle), and 3 (square). Values of parameters for each region given in Table S1. See text for parameter values.

Equations 8 and 9 indicate the dynamic system behavior can be entirely defined by the dimensionless parameters κ_R, κ_D, n_R, n_D, τ, and $\mathcal{V}_i$. We used the linear stability criteria for the classical case (Table 1) to calculate any VEGF concentration that would result in a MLE of zero any combination of parameters κ_R and κ_D. We defined this concentration as a "critical VEGF concentration" that changed the stability of the system from positive to negative, or vice versa, and constrained the possible values for VEGF concentration of our model (V_i) to reflect the VEGF concentrations that are known to stimulate angiogenesis from patient rumor samples [38].

Figure 6 *A* shows how the critical VEGF concentration depends on the parameters κ_R and κ_D for the nominal case where $n_R = n_D = 2$, and $\tau = 1$.The black

lines give the contours of VEGF concentration over the surface; these contours overlap, suggesting that certain systems will switch stability twice as VEGF is titrated into the system.

The analytical stability criteria accurately predicts when simulated differentiation occurs

The surface of critical stability shows three regions of behavior, marked 1-3 on Fig. 6 *A*. To understand the switching behavior of each region, we numerically integrated the nondimensional ODES (Eqs. 8 and 9) using a sample parameter combination from each region of the surface.

Figure 6 B shows the simulated differences between the highest and lowest Delta-expressing cells in a hexagonal lattice for each parameter pair. Region 1 $\{\log \kappa_R = -1.242, \log \kappa_D = -1.616\}$ shows the anticipated result that the system becomes unstable and patterns above a threshold concentration of VEGF. Region 2 $\{\log \kappa_R = -1.348, \log \kappa_D = -4.04\}$ shows the opposite result: the system is unstable under low concentrations of VEGF and becomes stable at the homogeneous state above a threshold concentration of VEGF. Region 3 $\{\log \kappa_R = -0.879, \log \kappa_D = -2.42\}$ is a combination of these two regimes in which there is a window of instability at intermediate concentrations of VEGF and stability at either extreme; this is where the contours overlap.

For the given parameter combinations, the spread of Delta expression (the maximum expression level observed divided by the minimum expression level

observed at the final steady steady-state) increased over unity above or below the VEGF concentrations predicted by the analytical stability criteria (Fig. 6 *B*), which were 10 pM, for regions 1 and 2. At the parameter combination labelled '3' in Figure 6 *A*, the Delta expression bifurcates at 3 pM and returns to stability at 31 pM. These precise concentrations have no physiological significance aside from being within the range observed in patient tumor samples [38], but this demonstration suggests that the analytical stability criteria is correct in determining when the full dynamical system will pattern based on the assumed kinetic rate laws and parameter values.

As such, Figure 6 *A* can be used to choose values for κ_R and κ_D that make the system pattern (or stop patterning) at any desired level of VEGF. Conversely, Figure 6 *A* can be used to constrain the appropriate combinations of κ_R and κ_D based on experimental observations of endothelial patterning in response to imposed VEGF concentrations, assuming the parameters n_R, n_D, and τ have already been estimated.

Cell network topology influences stability and final pattern

The purpose of this study was not only to determine the stability of the homogeneous steady-state, but also to predict what sorts of final patterns will form for an HSS-unstable system. Patterning of the system could be simulated for any tessellating geometry by changing the connectivity matrix *M* to reflect the appropriate network topology (Fig. 3). Figure 7 shows the patterned steady-state of the endothelium under the classical GRN in three ideal geometries: triangular, square, and hexagonal.

Qualitatively, the patterns of each geometry are "close-packed", in that tip cells (red) are as close as possible without having two tip cells be immediate neighbors. This result is notable because it suggests that tip cells will be very close to one another after tip-stalk selection occurs; if every tip cell becomes an angiogenic sprout, the initial vasculature will be pathologically dense under this regime.

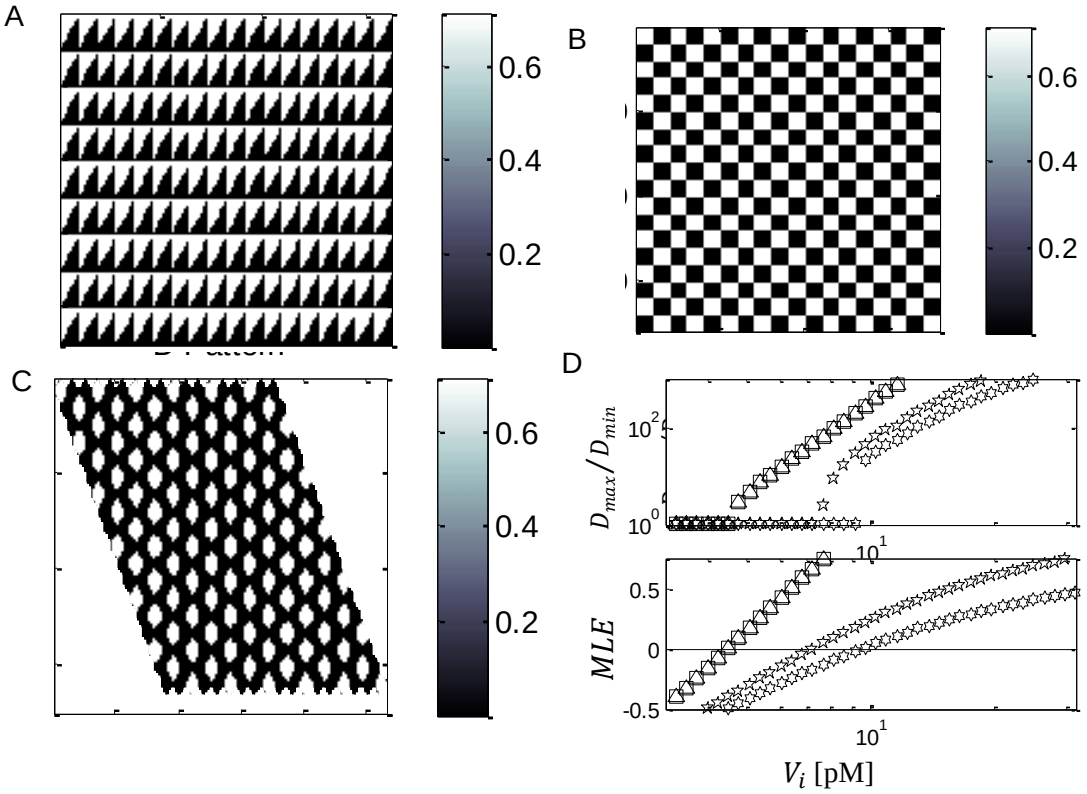

FIGURE 7 The final patterned states of Delta expression (white is a tip cell) for various lattice geometries (*A*, triangular; *B*, square; *C*, hexagonal) are qualitatively robust to noise in VEGF and close packed in each case. (*D*) The quantitative threshold for instability is influenced by the choice of geometry: the VEGF concentration required for patterning in higher in the hexagonal (6p star) and pentagonal (5p star, *pattern not shown*) geometries than in square (square) or triangular (triangle) geometries. The MLE, given by the analytical stability criterion (Table 1), correctly predicts the VEGF concentration required to induce patterning in the full dynamical system for each geometry.

The choice of geometry influences the stability criteria through the structural eigenvalue q_k, with hexagonal lattices having greater inherent stability than pentagonal (*not shown*), square, or triangular lattices. Fig. 7 *D* shows how the VEGF required to induce patterning shifts with the choice of geometry due to changes in q_k. The congruence between the analytical (MLE) and numerical results (D_{max}/D_{min}) indicate the linear stability criterion has a correct dependence on the cell network topology.

Tip-stalk patterning in non-uniform distributions of VEGF

The assumption made in most of these exercises is that both the endothelium and surrounding VEGF profile are uniform at the initial condition; this allows us to find whether the endothelium is capable of breaking symmetry in the manner of Turing. However, VEGF distributions in the interstitial fluid may be highly non-uniform in some cases: localized sources of VEGF from nearby tissues (or tumors) might concentrate VEGF in one area of the vessel, or heterogeneities in the VEGF binding

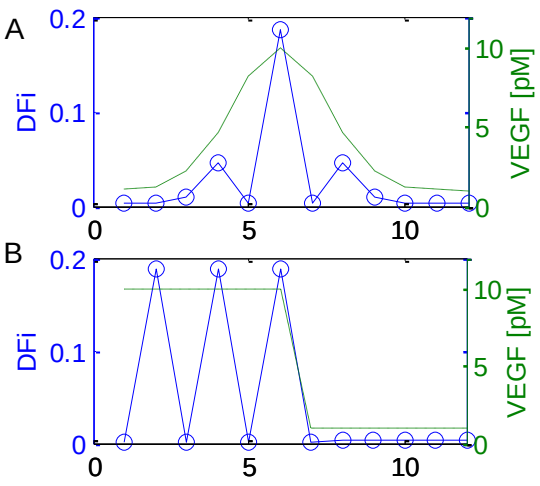

FIGURE 8 (*A*) High Delta expression can be localized to a single cell if the VEGF profile is sufficiently narrow (σ = 1.5 cells). (*B*) Local instability and patterning does not transfer to connected regions with low VEGF.

affinity and microstructure of the extracellular matrix may route VEGF to select few cells. We simulated the response of an endothelium to a localized source of VEGF using a Gaussian distribution (Fig. 8 *A*), and examined how patterning might spread around a vessel that is exposed to VEGF on a single side (Fig. 8 *B*).

It was observed that cells will form a normal close-packed pattern for all but the narrowest distributions of VEGF. A 10-fold increase in VEGF with a standard deviation of 1.5 cells led to a single high-Delta expressing tip cell with moderate-Delta expressing second-neighbors (Fig. 8 *A*). This indicates heterogeneities in VEGF distribution need to be both steep (high magnitude) and sharp (low std. dev.) to produce tip candidates with no second-nearest neighbor competitors.

Furthermore, a sharp transition in extracellular VEGF produces a similarly sharp transition in patterning potential under the classical stability criteria (Fig. 8 *B*); the pattern did not spread beyond the immediate influence of high VEGF.

Qualitative patterning differences between the hypothetical GRNS

Some authors have proposed changes to the basic Delta-Notch lateral inhibition mechanism that might shape tip-stalk patterns in the developing vascular plexus [7], and we investigated the patterning results of several of these hypothetical phenomena. Each hypothetical GRN was made to be unstable by the criteria in Table 1 and simulated in MATLAB. All GRNs except "Delta Feed-Forward" (Fig. 1 *B iii*) produced qualitatively identical final steady-states as Fig. 7 (i.e. the spacing of tip cells), although the speed of the response and the expression levels of each phenotype varied between GRNs.

The kinetic rate laws (Eqs. 18 and 19) derived from our interpretation of "Delta Feed-Forward", as described by Caolo, *et al.* [24], resulted in a stability criterion that had a positive dependence on the structural eigenvalue (q_k), unlike the other GRNs. This implied that the system would never be unstable on the negative structural modes that produce patterning in the other GRNs. In the numerical simulations, unstable homogeneous steady-states under the "Delta Feed-Forward" GRN synchronously moved from one homogeneous steady-state to another, implying that instability results in a uniform change in phenotype rather than patterning. This result contrasts with the other GRNs, where instability of the single available homogeneous steady-state resulted in heterogeneous differentiation.

We were uniquely able to achieve an oscillating tip-stalk pattern under the "Regulated Notch" regime by using a slow decay rate for the Notch receptor (γ_N in Eq. 17). The core lateral inhibition mechanism was faster than the up-regulation of Notch in highly VEGFR2-activated cells, so tip cells eventually accumulated enough Notch receptor to revert them back into the stalk phenotype characterized by low Dll4 and VEGR2 expression. Figure 9 shows an endothelium undergoing oscillations that displays an inverted pattern (individual stalk cell surround by tip cells) for portions of

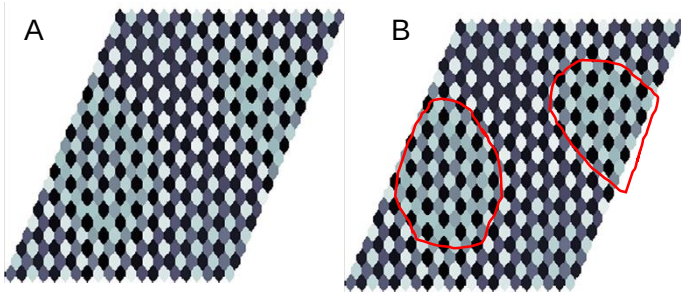

FIGURE 9 The endothelium temporarily anti-patterns during oscillations in the "Regulated Notch" regime after tip cells accumulate enough Notch receptor. The anti-patterned regions, circled red in *B*, will quickly revert to a normal tip-stalk pattern. Tip cells are white.

the lattice; this is caused by the accumulation of Notch in tip cells. This oscillatory pattern inversion represents a novel prediction about dynamic patterns of Notch activation in endothelial cells, and might help explain the finite lifetime of tip cell phenotypes observed in the live microscopy of *in vitro* angiogenesis [46].

Sparse patterning by lateral inhibition requires long-distance signaling

Close patterning (as close as possible without two neighbors being tip cells) using a standard network topology (Fig 2 *A* & *B*) was observed for every variation of the GRN that exhibited patterning, and it is not clear that this represents a healthy response in all cases of angiogenesis. The developing mouse retina contains a high density of tip cells at the advancing front [4], but assays involving embryoid bodies [25] and excised aortic rings [46] showed that stereotypical branching angiogenesis selects relatively few tip cells. In a related context, previous authors [6] have observed Delta-Notch patterns in 2D monolayers of cells that are highly sparse in comparison to the typical lateral inhibition patterns of Fig R4. The researchers, who observed the patterns in the epithelium of developing *Drosophila*, concluded that primary cells (tip cells in our model) were using filopodial extensions to increase the effective range of the cell membrane.

If tip-stalk patterning determines the sprouting density and branching frequency of angiogenesis, we should anticipate how sparse patterning of tip cells might be achieved in 2D layers of endothelial cells. To achieve sparse patterning, we incorporated longer-range juxtacrine signaling into our connectivity matrix (Fig. 2 *C*), an approximation of the static filopodia from Cohen, *et al.* [6]. Figure 10 shows the

spacing of tip candidates when long range signaling was approximated with $\varepsilon = 0.2$ (Eq. 22) under the classical GRN (Fig. 1 *B i*), implying that second nearest neighbors communicated with 20% of the strength of nearest neighbors.

Including long-range signaling in the connectivity matrix significantly lowered the minimum structural eigenvalue (q_k), making the systems more resistant to patterning. For example, a square array with $\varepsilon = 0.2$ had a minimum structural eigenvalue of $q_k = -0.66$ versus $q_k = -1$ for $\varepsilon = 0$. As such. achieving patterning at a reasonable concentration of VEGF with extended juxtacrine signaling required a much lower dissociation constant for VEGFR2 regulation ($\log \kappa_R = -2$) than in the control case $\varepsilon = 0$ ($\log \kappa_R = -1.242$) for the classical GRN, indicating that cells needed to be more sensitive to Notch signaling.

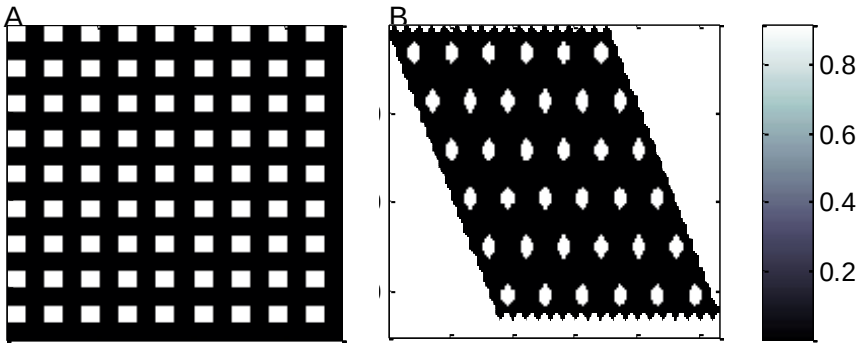

FIGURE 10 More sparse patterning can be achieved with ε = 0.2 in both square (*A*) and hexagonal (*B*) lattices. In *A*, a cell can contact its diagonal neighbors, while in *B*, a cell can contact its 12 second-nearest neighbors (see Fig. 2 *C*).

CHAPTER 5

DISCUSSION

Analytical results and theory

Some vascular biologists hypothesize that the spontaneous differentiation of tip and stalk phenotypes from a uniform endothelium after exposure to VEGF predetermines the location or density of angiogenic sprouts [47]. Experiments have suggested that signaling from the highly conserved Notch receptor drives this heterogeneous differentiation by sensing and regulating the expression of Delta-like ligand 4 and VEGFR2 [5].

In this paper, we formalized the hypothesized core "classical" regulatory interaction between VEGFR2, Delta, and Notch (as well as several experimentally supported variations of the GRN) to determine if and how the lateral inhibition control loop could result in the patterning of cell phenotypes using a linear stability analysis in the tradition of Turing [29]. The result of this analysis are mathematical criteria (Table 1) that the hypothetical gene regulatory networks must satisfy to produce patterning if the empirically observed interactions (e.g. Notch signaling down-regulates VEGFR2 expression) are approximated as Hill functions.

Stability depends on gene regulatory and signaling topology

The criteria for instability and patterning in each variation of the GRN is listed in Table 1, but let us examine the "classical" criteria in detail. The product in the

Maximal Lyapunov Exponent (MLE, the left hand side of every stability criteria in Table 1) that contributes to instability ($-q_k n_R n_D g_R g_D$) incorporates information about the steady-state expression levels of the regulators that drive lateral inhibition (g_R and g_D, can also be represented as $1-\mathcal{R}_{ss}$ and $1-\mathcal{D}_{ss}$), the Hill coefficients of those regulators (n_R and n_D), and the structural mode on which the pattern will form ($-q_k$). In this way, the linear stability analysis incorporated information about the topology of signaling across the local tissue and the intracellular gene regulatory landscape at the homogeneous steady-state.

As seen in Fig. 6, exogenous VEGF induces instability and patterning in the classical case by changing the MLE from negative to positive; it does this by altering g_R and g_D, which are functions of the steady-state expression levels of VEGFR2 and Delta. The VEGF concentration at which pattern occurs is not constant among different lattice geometries (Fig. 7 *D*) because the minimum structural eigenvalue (q_k) ranges from -1 for linear arrays of cells, square lattices, and triangular lattices; to -0.5 for hexagonal lattices.

In a physical sense, the structural eigenvalue represents the wavelength of the spatial pattern (see Othmer & Scriven [30] for a discussion of structural eigenvalues and eigenvectors in regular lattices): a larger negative eigenvalue indicates a denser pattern in the tissue, meaning that neighboring phenotypes will bifurcate in opposite directions, resulting in a "checkerboard" pattern. Larger negative eigenvalues are the most unstable modes in the models presented here; this indicates that all the hypothetical GRNs underlying tip stalk selection will have an intrinsic preference for

forming fine grained patterns in the absence of longer-distance juxtacrine signaling. The exception is "Delta Feed-Forward", which only becomes unstable for large positive structural eigenvalues, which correspond to phenotype excursions that are uniform over the entire lattice. This is not patterning.

Patterning requires cooperativity

As mentioned earlier, the upper limits on the product of g_R and g_D and the predetermined minimal values of q_k for a given lattice together require the product of the Hill coefficients to exceed a certain value ($n_R n_D > 2$ for a hexagonal lattice) for instability and pattering to be possible under any circumstances. Other researchers have arrived at this same conclusion and considered it to be evidence that mechanisms other than simple lateral inhibition are necessary for pattern formation by Delta and Notch, citing as evidence that the measured cooperativity (Hill coefficient) between the Notch Intracellular Domain and CSL promoter is $\sim 0.7 - 1.6$ [32].

However, the present study has shown that no single mechanism needs to have exceptionally high cooperative action, but rather that full gene regulatory network needs to have effective cooperativity or nonlinearity. The effective cooperativity may arise from futile cycles in the downstream phosphorylation pathways of VEGFR2, from nonlinear signaling rate laws with respect to Notch and VEGFR2, or from any reaction that occurs "in series" with the classical lateral inhibition control loop (Fig. 1 *B i*). Indeed, an exponent added to the concentration of VEGFR2 (n_a) in our kinetic rate law for VEGFR2 signaling (Eq. 23) is included in the final product of exponents ($n_R n_D n_a$) in our stability criteria (Table 1) and aides in pattern formation.

Different hypothetical GRNs have differently structured stability criteria

The alternative hypotheses about the GRN underlying tip stalk differentiation (Fig. 1 *B*) had more complicated stability criteria because they altered the structure of the lateral inhibition control loop (Table 1).

The addition of basal expression to the classical GRN (Fig. 1 *B i*) results in a diminished capacity for patterning by scaling down the unstable term ($-q_k n_R n_D g_R g_D$) by the fraction of steady-state expression that is basal expression ($\left(1-\frac{\alpha_R}{R_{ss}\gamma_R}\right)\left(1-\frac{\alpha_D}{D_{ss}\gamma_D}\right)$). This is an intuitive result because adding expression that is constant across the tissue would make it harder for any mechanism to break the uniformity of the HSS. This result has implications for the application of lateral inhibition patterning to synthetic biology, where regulatory elements are expected to have measureable leakage.

The stability criterion for 'Regulated Notch' (Fig. 1 *B ii*) has a separate term that represents the intracellular control loop that regulated Notch expression based on VEGFR2 signaling. This second loop is summed with the original criteria because it is parallel to the lateral inhibition loop. It also does not factor in the structural eigenvalue because it does not involve Delta-Notch signaling. The sign of the second term is negative, so it has the effect of making the system more stable. As seen in Figure 5, the 'DNDT' nullcline has a more gradual slope with less extreme minimum and maximum, meaning the system is closer to having only one possible steady state. The addition of 'Regulated Notch' may prevent systems from patterning if the decay rate

(γ_N) or cooperativity (n_N) of Notch regulation are sufficiently high (Table 1). In essence, the lateral inhibition feedback loop must have a greater cooperativity than the Notch-VEGFR2 feedback loop.

The hypothetical regulatory network behind 'Delta Feed-Forward' (Fig. 1 *B iii*) has lost its capacity for lateral inhibition. Because Notch signaling effectively induces both the tip and stalk phenotypes, neighboring cells are unable to inhibit their neighbors from responding to VEGF while retaining their own capacity to respond to VEGF. This is reflected by the lack of instability for large negative structural eigenvalues that correspond to fine-grained patterning.

The criterion for the GRN that includes VEGFR1 (Fig. 1 *B iv*) is more complicated because it involves multiple modes of juxtacrine signaling, but it follows the same logic as the other criteria. The lateral inhibition term ($-q_k n_R n_D g_R g_D$) is conserved, but an additional term allows the effects of VEGFR1 expression in stalk cells to enhance the selection of tip and stalk cells. However, if sVEGFR1 is too diffuse (large K_S), then the addition of VEGFR1 expression does not contribute to the formation of a pattern, as all cells experience the same inhibitory effect.

The logical relationship between the structure of the GRN and the form of the stability criteria is consistent with the 'open-loop transfer functions' of chemical process control, suggesting a future possibility for elucidating system behavior directly from flow diagrams of the gene regulatory networks and transfer functions that model node behavior [48].

Quantitative and numerical aspects

Though we lack reliable estimates for many of the parameters used in our model, the small number that remained after non-dimensionalization allowed us to map most of the qualitative behaviors that the system could possibly exhibit. From these qualitative observations, we can back out how the quantitative aspects of our model influence patterning.

The dimensionless forms of the classical GRN (Eqs. 5 and 6) had a limited set of parameters (κ_R, κ_D, n_R, n_D, τ, and V), constraining the independent variables on which the range of system behavior is dictated. After setting the effective Hill coefficients (n_R and n_D) each to 2 and assuming the degradation rates of Delta and VEGFR2 were equal ($\tau = 1$), the analytical stability criteria for the classical case was used to find critical VEGF concentrations that resulted in marginal stability (MLE = 0) while the dissociation constants for gene expression (κ_R and κ_D) were varied.

Figure 6 *A* shows that two essential system behaviors are determined by these dimensionless parameters: (1) The VEGF concentration at which the system switches stability, and (2) the quality of the switch-like behavior at the critical VEGF concentration.

Influence of the effective dissociation constants

Numerical simulations confirmed the analytical stability criteria correctly predicts when the classical GRN will start to pattern (Fig. 1 *A ii*). If our model for the GRN underlying tip-stalk differentiation is accurate, we can possibly arrive at estimates for

the parameters κ_R and κ_D by subjecting *in vitro* monolayers of endothelial cells to a titration of VEGF and observing if and when the cells start to heterogeneously differentiate. A tissue-scale pattern of gene expression could, in principle, be observed after immunocytochemical staining for either DLL4 or VEGFR2, or the differentiation could be measured by looking for a splitting of phenotypes using flow cytometry.

Influence of the effective Hill coefficients

The dependence of pattern formation by lateral inhibition on high levels of effective cooperativity motivates us to measure the effective Hill coefficients underlying the gene regulatory networks. Previous researchers measured the Hill coefficients of specific transcription factors downstream of Notch [32], but fitting a Hill function to an entire GRN path remains a challenge. It may be possible to grow endothelial cells *in vitro* and measure their relative expression of Delta as VEGF is titrated into the system, and similarly we might be able to relate VEGFR2 expression to imposed concentration of Delta ligand [32]. These experiments, though likely exhibiting much variability, may give us some insight into the sharpness of the transition to tip and stalk phenotypes when VEGF is introduced into a system, and tell us whether their capacity to pattern is robust.

Effects of hypothetical GRN variations

One purpose of this study was to determine what effect the intracellular topology of the gene regulatory network (that is, the set of dynamic genes/species and their interactions) had on the qualitative and quantitative aspects of tip-talk selection.

Understanding how sensitive our predictions are to uncertainty about the GRN topology is crucial because it is still not clear if the same species are used in every context (e.g. *in vitro* angiogenesis versus embryonic development) in the same way [24].

As is evident in Table 1, variations in the hypothetical GRN topology led to different stability criteria, which established different requirements for the HSS to become unstable and pattern. Some variations had an easier time patterning ("VEGFR1 expression", Fig. 1 *B iv*) because they reinforced the lateral inhibition mechanism, while others were resistant to patterning because they fought lateral inhibition ("Regulated Notch, Fig. 1 *B ii*).

These differences in stability criteria help us understand how the angiogenic activity might be differentially regulated in different tissues or stages of development, but they do not yet offer us a method of excluding one mechanism or another in a given context because we do not have accurate parameter estimates for κ_R and κ_D, which are strongly dependent on the choice of GRN. Instead, qualitative differences in patterning are our best bet for excluding each GRN for a given context.

For instance, the "Regulated Notch" regime would result in a spatial pattern of Notch expression similar to those in Figure 7, as Notch expression should be correlated to VEGFR2 or Delta expression. The lack of spatially periodic Notch expression would suggest that Notch expression is constant.

Or, if VEGFR1 expression is essential for pattern formation in an endothelial monolayer, the RNA silencing of VEGFR1 should stabilize the HSS and prevent patterning; or at least, increase the level of VEGF required to induce patterning.

We have excluded "Delta Feed-Forward" as a principle mechanism behind the selection of tip and stalk cells. While the authors that proposed this mechanism [23] gave a reasonable explanation of how the signaling pathways of VEGFR2 and Notch intersect, our interpretation of their proposed GRN cannot perform lateral inhibition. The literature strongly suggests that NICD can promote the expression of Delta ligand, but lateral inhibition requires that VEGFR2 must be able to modulate Delta expression independently of Notch signaling. The GRN used here may help explain how uniform Delta expression is maintained across quiescent vascular tissues, as observed in adult arteries [23].

Quantitative certainty about the values of any of our parameters is not yet achievable because the experiments that suggested each of these hypothetical GRNs are loosely united. Further research, with carefully defined experimental parameters and procedures, will be needed to assemble a mathematical model with the accuracy that can differentiate between each GRN with quantitative accuracy.

Qualitative pattern formation

Switch-like behavior can go either way

Some of the earliest and most influential descriptions of VEGF describe it as critical factor in tumor-induced angiogenesis [15, 49], and this would suggest a role of

elevated VEGF in destabilizing the homogeneity of the adult vessel. We used the criteria for instability to find how VEGF might switch the stability of the homogeneous steady-state of differentiation in the classical GRN (Fig. 1 *B i*). The classical criterion of Table 1 was used to find concentrations of VEGF that resulted in an MLE of zero, corresponding to a switch in HSS stability (as an eigenvalue passes the origin), for each combination of parameters κ_R and κ_D.

The resulting surface of critical VEGF concentrations, shown in Figure 6, predicts that instability and pattern formation can be switched either on or off by increasing VEGF. For some combinations of κ_R and κ_D, patterning is only induced for a specific window of VEGF concentrations. However, the phenomena of stability at high concentrations of VEGF is probably not physiologically realistic under this formalism.

Vascular networks formed under pathologically high VEGF are tortuous, dilated, and covered in filopodia [4, 50], which would suggest the uniform selection of tip cells; however the uniform expression levels of Dll4 and VEGFR2 under high VEGF concentrations are extremely low in the model presented here. A real-life endothelium with uniformly low VEGFR2 expression levels would certainly not productively sprout, but it would not have filopodia either based on our definition of a filopodia-expressing tip cell (high VEGFR2 activation). This discrepancy might suggest a need to include a basal VEGFR2 expression rate (Eq. 15) so that at least some VEGFR2 activation is present under pathologically high levels of VEGF. Future experiments will hopefully clarify if endothelial tissues indeed maintain patterns of

Notch signaling (or VEGFR2/Delta expression) for limited windows of VEGF concentration, and how the bulk VEGFR2 expression levels change under pathologically high VEGF.

Final pattern spacing is robust to noise, parameter values, even kinetic rate laws

One possible application of this model is to predict the initial density of angiogenic sprouts from an endothelial monolayer by determining the patterns of tip cells formed under specific experimental conditions. To estimate the range of patterns this model was capable of generating, each variation of the GRN was numerically simulated in a regulated lattice of cells. For systems that were determined to be unstable by the linear stability criteria (Table 1), all simulations reached the steady-state patterns depicted in Figure 7 regardless of the GRN used or values of individual parameters.

The only exceptions were for lattices with periodic boundaries that did not permit a uniform pattern (most noticeable for small grid sizes), and for long-distance Delta-Notch signaling as shown in Figure 10. For the former exception, the pattern takes on a polycrystalline structure with "grains" of close-packed patterns separated by visible faults. This is likely a consequence of the artificially perfect lattice, because a biological monolayer of cells is disordered enough (individual cells have 5 – 7 neighbors) to blur the patterns away from perfect crystallinity [6].

Sparse patterning, on the other hand, was deliberately introduced by including longer range interactions into the connectivity matrix (Fig. 2 *C*). In this altered topology of the cell network, individual cells sampled second-nearest neighbors with a

scaled weight ε when determining the neighboring Delta concentration, as in Eq. 22. The result is that tip cells space themselves out to a greater degree to avoid having other tip cells in their neighborhood (Fig R5), effectively reducing the number of tip cells selected by lateral inhibition and increasing the cellular distance between potential sprouts.

The biological mechanism that would result in effectively longer-range Delta-Notch signaling in planar endothelial cells is currently unknown, but recent studies have suggested that filopodia acting as cytonemes may extend the membrane border of cells in certain networks [6], or that endothelial migration transiently "shuffles" the topology of the network as cells dynamically compete for the tip phenotype [28].

The rule of topology

The strong dependence of the final pattern on the cell network topology is crucial because it suggests tissue-scale interactions as a key factor in pathological hyper-sprouting as opposed to just local morphogen (VEGF) concentration. Previous theoretical and computational studies of pattern formation by juxtacrine lateral inhibition all arrived at the conclusion that lateral inhibition cannot produce spatial patterns on a wavelength greater than two cells [8, 22], corresponding to the close-packed patterns of Figure 7.

Recently, combined computational and experimental studies have begun to explore how specific changes to the intracellular GRN determine the effective topology of the signaling network and control pattern formation, for instance by

depleting the surface-bound Notch and Delta of certain cells through mutual inactivation [32]. This has the effect of removing the either 'sending' or 'receiving' capabilities of nodes in the lattice, altering the effective topology.

In addition, it has been proposed that lateral induction by juxtacrine signaling can produce patterns on a wavelength greater than two cells [53], but it is not clear that endothelial tip-stalk differentiation includes GRN motifs that resemble this mode of differentiation (Notch signaling would need to induce Notch expression as well as Delta expression for this framework to apply – this has not been observed).

The dominance of topology in determining emergent biological behavior has been proposed as a general rule in systems biology [51, 52], but this study and others have confirmed that the numerical details of the intracellular GRN still determine if and when a patterning event can occur (i.e. the criteria for instability). The uncertainty that remains about the GRN that most accurately predicts tip-stalk differentiation in the context of adult angiogenesis motivates using well-defined *in vitro* experiments on primary endothelial cells to answer some questions raised by this study.

The breakdown of symmetry in the endothelium

The results this far have shown that the VEGFR2-Delta-Notch regulatory architecture can theoretically produce spatial patterns of tip and stalk cells from an initial condition that is uniform in both phenotype and extracellular VEGF. Under these assumptions, a uniform increase in extracellular VEGF concentration leading to the spontaneous formation of a multicellular pattern would mark the first steps toward vascular

morphogenesis as cells break the symmetry of the endothelial monolayer. However, there are contexts where the assumption of initial uniformity is more or less appropriate.

In vitro studies that seek to recapitulate sprouting angiogenesis often start by culturing cells under quiescent conditions on chemically and mechanically uniform collagen scaffolds [2, 41]. The initial conditions of these experiments closely match those of our model, and any multicellular structures that form after the introduction of VEGF *in vitro* are the result of broken symmetry by cell signaling and differentiation. Similarly to our model predictions, sprouts previously formed in these *in vitro* model systems might be considered pathologically dense by *in vivo* standards [54].

In the adult, the endothelial cells of a large vessel might be uniform in phenotype under normal conditions, but are subjected to heterogeneities in the surrounding microenvironment that might influence the site of sprout initiation in response to hypoxia, including pericyte coverage and localized sources of VEGF (tumors). Interestingly, the experimental origin of tip-stalk selection is the context where its role in determining sprouting density might be the most compromised: the developing mouse retina contains a pre-existing pattern of VEGF, laid down by migrating astrocytes, which endothelial cells follow to establish a vascular plexus [4].

The extent to which the gene regulatory interactions of tip-stalk selection play a role in the *de novo* self-assembly of vascular sprouts in applications of tissue engineering remains a mystery. To answer this question, we shall propose a set of

experiments to test the patterning of tip and stalk phenotypes (as defined by their gene expression) in initially uniform endothelial monolayers.

CHAPTER 6

FUTURE WORK

Expression patterns of VEGFR2 and Delta-like ligand 4 in the endothelium

The mathematical model presented in this paper predicts that tip cells will differentiate from a planar endothelium under the influence of VEGF at relatively high numbers compared to previous in vitro assays of branching morphogenesis [2, 25, 46, 54]. Under the most basic assumptions about the topology of the lattice, 1/3 (in a hexagonal lattice) to 1/2 (in a square lattice) of endothelial cells will adopt a tip phenotype as defined by the elevated expression of Dll4 and VEGR2. Furthermore, tip cell can be identified by their extension of filopodia, which are focal points of VEGFR2 expression [4]. It is possible that, upon subjecting a monolayer of endothelial cells to VEGF (and other controlled reagents), we will be able to estimate the spacing of tip cells using *in situ* microscopy; or, we could measure the ratio of low- and high-Dll4 (or VEGFR2) expressing cells (for instance by flow cytometry) to arrive at an estimate for tip cell density.

If tip cells are close-packed like the classical model predicts, it would suggest the VEGFR2-Delta-Notch regulatory framework indeed produces many tip candidates and that subsequent angiogenic phenomena (e.g. sprout elongation, anastomosis, or pruning) are needed to produce a vascular plexus with the expected sprout density and branching frequency [2, 25, 46, 54]. If tip cells are present in low numbers and are spaced far apart, it would support the possibility that as-of-yet unknown biological

mechanisms alter the effective topology of the cell network to extend range of lateral inhibition. A situation where no clear pattern of VEGFR2 or Delta expression emerges prior to the outgrowth of sprouts would suggest that other phenomena determine how the uniform monolayer breaks symmetry and self-assembles into sprouts.

The results of these preliminary experiments would motivate either a broader literature search for the gene regulatory and biophysical mechanisms of endothelial differentiation that lead to sprout initiation, or more intensive laboratory work to study the dynamics and control of tip-stalk differentiation within the VEGFR2-Delta-Notch framework.

Dynamics of Notch signaling in the endothelium

If *in vitro* endothelial monolayers form close-packed patterns as predicted by the GRNs considered here, we shall probe deeper into experiments about the dynamics and steady-states of endothelial patterning. An attractive method for characterizing tip-stalk selection would involve a live reporter of Notch signaling. Previous studies have used Notch signaling reporter plasmids to probe the spatial distribution and dynamics of Notch activity with considerable success [4, 39].

These plasmids work by incorporating a tissue responsive element (TRE) in the promoter region of a sequence that encodes a molecular reporter, such as luciferase or green fluorescent protein (GFP). This TRE is suppressed by the *RBP-Jk* complex, which can bind to NICD after the Notch receptor is activated, allowing transcription to occur; in effect, Notch signaling activates the expression of a reporter. Researchers in

previous studies made Notch reporter plasmids from scratch, but at least one company now offers a lentiviral Notch signaling GFP reporter for sale [55].

We could use such a virus to transduce the reporter plasmid into a primary cell line and observe the dynamic signaling of Notch in an endothelial monolayer or 3D culture using live microscopy. This would allow us to see oscillations (as suggested by the 'Regulated Notch' GRN), characterize the Notch activity of a multicellular sprout, or elucidate the time scales over which endothelial cells pattern. Measureable time scales would help us refine the model and inform which molecular mechanisms are most important for robust patterning. For instance, one study suggests that VEGFR2 transiently up-regulates Delta through the Tel/CBP complex for only 40 – 60 minutes after the introduction of VEGF [33]. The holistic nature of this readout makes it the best option for probing systems biological questions related to tip-stalk pattern formation.

Model fitting

This model currently predicts bifurcations in Delta expression that are not likely physiological, with the ratio between the minimum and maximum Delta expression being on the order of 100-fold change (Figure 6). A first stop in getting this model ready to quantify endothelial differentiation will be to get the model predictions to within reasonable levels. While *in situ* micrographs of endothelial patterning are not widely available, we might estimate that the phenotypes will differ by closer to an order-10-fold change in gene expression [4]. We need to determine if the model can achieve a pattern with this degree of separation.

We may also be able to get our model closer to quantitative accuracy by recapitulating key interventions made by previous experiments. Some studies measured changes in expression of VEGFR2 and Delta in response to VEGF in endothelial cultures [10], while others have looked at the same species before and after the inhibition of Notch signaling [25]. While these experiments may not be able to determine the relative transcript and protein levels in individual tip and stalk cells because they rely on bulk property measurements, we can simulate the bulk property measurements by averaging over our cellular lattices.

While this study mostly focused on steady-states and their stability, we have uncovered some possibly interesting dynamics that endothelial cells might exhibit as they respond to VEGF. We will gather more accurate estimates for the response times of each step in our model from previous experiments to make reasonable estimates for various characteristic times. For instance, with more accurate knowledge about the decay rate of VEGFR2 and Delta, we may establish a number of hours needed to pattern under 'Regulated Notch' versus 'VEGFR1 expression' and get a sense for which is most accurate.

GRN validation

We have excluded "Delta Feed-Forward" as a possible GRN that enables tip-stalk selection in the endothelium because it was unable to produce spatial patterns. However, three GRNs remain: the classical GRN (Fig. 1 *B i*), the "Regulated Notch" GRN (Fig. 1 *B ii*), and the "VEGFR1 Expression" GRN (Fig. 1 *B iv*). We can only exclude these GRNs in specific contexts by directly testing their assumptions in those

specific contexts. A context might be the patterning of HUVECs cultured on Type I Collagen.

For instance, if VEGFR1 is upregulated by Notch signaling, we should see an increase in VEGFR1 expression when we subject HUVECs to a titration of extracellular Delta. Sprinzak, *et al* [32] devised a method for subjecting cells to controlled levels of Delta, and we could employ their technique in conjunction with immunfluorescent staining or other methods to measure to response curve of VEGFR1 (or any species in our model) with respect to Notch signaling. If there is a Hill-like response, we then need to show that VEGFR2 signaling is affected by VEGFR1 expression. Previous literature suggests this occurs [42], but we could confirm it ourselves. A failure to show any of these effects would indicate that the "VEGFR1 Expression" GRN is not appropriate for determining tip-stalk patterning in HUVECs.

Similarly, we should be able to show a Hill-like response of Notch to VEGF stimulation if "Regulated Notch" is correct. It may be easier to see this effect if Notch signaling is inhibited to prevent tip-stalk patterning from introducing heterogeneous VEGFR2 expression. A lack of change in Notch expression in response to VEGF would cast doubt on "Regulated Notch" as an appropriate GRN.

Finally, we need to clearly see the down-regulation of VEGFR2 in response to extracellular Delta, and the up-regulation of Delta in response to VEGF. Unlike previous studies which often attempted to establish these relationships without consideration of tissue patterning, we will perform our experiments with a respect of

the possibility of broken symmetry to prevent it when desired, for instance by inhibiting Notch signaling.

Expanded species consideration

In the event that preliminary experiments are not supportive of VEGFR2-Delta-Notch pattern formation in primary endothelial cells under any GRN, we will need to expand our model framework. The species included in this GRN variations study by no means completes the list of pathways that are known to interact with endothelial cells during tip-stalk selection and angiogenesis.

Some pathways that are known to influence tip-stalk selection during development are VEGFR3, which is present in vascular endothelial cells during early development and regulates Delta expression; Jagged1, which is a ligand for Notch that may inhibit signaling to reinforce tip phenotypes; and BMP/Smads, which can activate Notch target genes independently of Notch [24]. Other studies have suggested kinetic rate laws for Delta-Notch signaling that alter the outcome of patterning: the 'mutual inactivation' suggested by Sprinzak, *et al* [32] was not included in this study because Dll1, not Dll4, was their subject. The different isoforms of VEGF were also not considered, nor were any other soluble growth factors that are known to contribute to angiogenesis, because it is still unclear at what stage of angiogenesis these additional morphogens become substantially involved.

The inclusion of these additional species or dynamic intermediate reactions with the VEGFR2-Delta-Notch framework would necessitate the use of more ODEs.

This would make traditional analysis more difficult and shift our approach towards the mainstream of multiscale modeling [56]. This shift may increase the capabilities and complexity of our model at the cost of its *intuitive* utility. This is a potentially problematic compromise, as the goal of any modeling effort that extends from the present consideration of tip-stalk selection will be to *intuitively* and functionally understand how an endothelial monolayer initially breaks multicellular symmetry.

Synthetic pattern formation

Aside from its physiological accuracy, this framework of multicellular patterning by juxtacrine signaling and receptor-ligand gene regulation presents an opportunity to revisit Turing's thesis of chemical morphogenesis [29].

A recent study observed the breakdown of symmetry in non-biological arrays of oil droplets that contain reagents of the oscillating Belousov–Zhabotinsky reaction [57]. Remarkably, this study occurred over sixty years after the publication of Turing's thesis, but it may be among the first experiments to confirm the basis of his theory about order in cellular arrays spontaneously arising from diffusive processes.

Turing intended his 1952 work to be the first of many prototypical computational simulations and only an abstraction of the biological processes that occur within cells, stating "Most of the organism, most of the time, is developing from one pattern into another, rather than from homogeneity into a pattern" [58]. However, with the advance of *in vitro* biology, which is constrained to initial microscale uniformity; and synthetic biology, which can engineer dynamic gene regulation with

precision, it will soon be possible to engineer Turing's biological pattern formation into living cells. The minimalist regulatory framework presented in this paper provides general design criteria for genetic circuitry that could produce the controlled breakdown of symmetry in mammalian cells, such as highly cooperative regulators and tunable dissociation constants (or production rates, depending on the nondimensionalization).

The foundation for this avenue of research has again been laid by Sprinzak, *et al*. [32] who transduced immortalized cells with a synthetic Notch signaling pathway that could control the expression of target genes. By coupling the expression of said target gene to the expression of a Notch ligand, it would be possible to generate *de novo* multicellular patterns in the manner described in this thesis. RNA-based regulators are inherently tunable and may be ideal substrate for the gene regulatory circuitry needed to destabilize a homogeneous steady-state. The bottom-up engineering of deterministic self-assembly (in the sense of increased order) in mammalian cells would be an impressive display of our current understanding of both systems biology and biomolecular synthesis.

CHAPTER 7

SUMMARY

This model formalized the empirical regulatory framework of endothelial tip-stalk differentiation by lateral inhibition, and suggested experiments that could evaluate tip-stalk selection as viable theory for the onset of vascular morphogenesis from uniform endothelium.

A linear stability analysis suggested key parameters that enabled the formation of a tip-stalk pattern: the effective cooperativity and dissociation constants of the gene regulatory interactions approximated as Hill functions were more critical than the response times. The topology of the cell signaling and gene regulation networks were found to determine the quantitative stability of the homogeneous steady-state endothelium, but the topology of the intracellular gene regulatory networks did not affect qualitative patterning results. Under the assumption that cell communication was limited to nearest neighbors in a lattice, patterning results were consistently dense; increasing the distance of juxtacrine signaling was the only way to change the number of tip cells selected. The exception was for the "Delta Feed-Forward" GRN, which was unable to form a spatial pattern of differentiation because it did not preserve the lateral inhibition motif.

The most pressing experiment inspired by this model is to determine if primary endothelial cells undergo Delta/VEGFR2 patterning in the presence of VEGF and other angiogenic cues. Following these preliminary results, this model framework will

provide a jumping-off point towards broader models of endothelial gene regulation, and deeper experiments into the *in vitro* self-organization of endothelial cells and beyond.

APPENDIX A1

DEVELOPMENT OF STABILITY ANALYSIS FOR A LATTICE OF CELLS

This is a derivation of the linear stability analysis for a generic system of lateral inhibition by Delta-Notch. It first assumes that generic functions f_R and f_D regulate the expression of VEGFR2 and Delta. The procedure begins after we have simplified the problem to two ODEs.

Following the quasi-steady-state assumptions for the kinetics of Notch and VEGFR2 signaling, the problem is reduced to two ODEs incorporating the rates of expression and degradation for VEGFR2 and Delta ligand in cell *i*.

$$\frac{dR_i}{dt} = f_R(\langle D_i \rangle) + r_R(R_i) \tag{A1.1}$$

$$\frac{dD_i}{dt} = f_D(R_i) + r_D(D_i) \tag{A1.2}$$

The *f* terms in these equations describe the rate of gene expression as a function of the gene in the argument. In this simplified view, they absorb the kinetics of signal transduction (f_D includes VEGF-VEGFR2 signaling and f_R includes Delta-Notch signaling) and in practice may resemble activating or repressing Hill-type functions. The argument of f_R references an average value of Delta expression $\langle D_i \rangle$ which is a sum of the Delta expression in cells neighboring cell *i*, as determined by

$$\langle D_i \rangle = \sum_j^v D_j \tag{A1.3}$$

where *v* is the number of cells in contact with cell *i*. Equations A1.1 and A1.2 also contain *r* terms which describe the decay of each species. At the uniform, non-equilibrium, steady-state (UNESS) corresponding to a homogeneous endothelium,

Equations A1.1 and A1.2 can be set to zero to determine the uniform, steady-state values of R_i and D_i, referred to as R_S and D_S.

$$\frac{dR_i}{dt} = \frac{dD_i}{dt} = 0 \; [UNESS]$$

$$\left.\begin{matrix} R_i \\ D_i \end{matrix}\right|_{UNESS} = \begin{matrix} R_S \\ D_S \end{matrix}$$

Let us define two deviation variables representing the departure of R_i an D_i from the UNESS, for instance following a minor perturbation.

$$x_1^i = R_i - R_s$$

$$x_2^i = D_i - D_s$$

To perform our linear stability analysis, we may substitute these variables into Equations A1.1 and A1.2 and perform a series expansion about $x_1^i = x_2^i = 0$, retaining only terms that are *O(1)* for small perturbations in *x*.

$$\frac{dx_1^i}{dt} = f_R(D_S) + \sum_j^v \left[\left(\frac{\partial f_R(\langle D_i \rangle)}{\partial \langle D_i \rangle} \right)_{\langle D_i \rangle = D_s} x_2^j \right] + r_R(R_S) + \left(\frac{\partial r_R(R_i)}{\partial R_i} \right)_{R_i = R_s} x_1^i$$

From the definition of the UNESS, it can be easily seen that the first and third terms cancel out, leaving only the terms first order in *x*. The same process can be applied to Eq. A1.2, leaving two linearized equations.

$$\frac{dx_1^i}{dt} = \sum_j^v \left[\left(\frac{\partial f_R(\langle D_i \rangle)}{\partial \langle D_i \rangle} \right)_{\langle D_i \rangle = D_s} x_2^j \right] + \left(\frac{\partial r_R(R_i)}{\partial R_i} \right)_{R_i = R_s} x_1^i$$

$$\frac{dx_2^i}{dt} = \left(\frac{\partial f_D(R_i)}{\partial R_i} \right)_{R_i = R_S} x_1^i + \left(\frac{\partial r_D(D_i)}{\partial D_i} \right)_{D_i = D} x_2^i$$

Notice the summation of neighboring Delta levels now occurs outside the function f_R. This is only appropriate because the system is now linear. The two ODEs for cell *i* can

be reduced to one by combining x_1^i and x_1^i into a vector $\boldsymbol{x}^i$ and rearranging the coefficients into matrices.

$$\boldsymbol{x}^i = \begin{pmatrix} x_1^i \\ x_2^i \end{pmatrix} \tag{A1.4}$$

$$\boldsymbol{K} = \begin{bmatrix} \dfrac{\partial r_R(R_i)}{\partial R_i} & 0 \\ \dfrac{\partial f_D(R_i)}{\partial R_i} & \dfrac{\partial r_D(D_i)}{\partial D_i} \end{bmatrix} \tag{A1.5}$$

$$\boldsymbol{B} = \begin{bmatrix} 0 & \dfrac{\partial f_R(\langle D_i \rangle)}{\partial \langle D_i \rangle} \\ 0 & 0 \end{bmatrix} \tag{A1.6}$$

where the partial derivatives of $\boldsymbol{K}$ and $\boldsymbol{B}$ are evaluated at the UNESS. In this matrix representation, the ODE governing the species of cell *i* becomes

$$\frac{d\boldsymbol{x}^i}{dt} = \boldsymbol{K}\boldsymbol{x}^i + \sum\nolimits_j^v \boldsymbol{B}\boldsymbol{x}^j \tag{A1.7}$$

where the first term can be thought of as the "intracellular term" governing all internal processes in cell *i*, while the second term can be considered the "transfer term" describing how neighboring cells interact through Delta signaling.

It will now behoove us to reformulate the problem in the method of Othmer & Scriven (1971), which combines all the vectors $\boldsymbol{x}^i$ for a network of *N* cells into a single vector-of-vectors $\boldsymbol{X}$. To achieve this, we define a tensor product of vectors $\boldsymbol{u}$ and $\boldsymbol{y}$ as follows:

$$\boldsymbol{u}\otimes\boldsymbol{y} = (u_1 y_1, \dots, u_1 y_n, \dots, u_N y_1, \dots, \dots, u_N y_n)^{\mathrm{T}}$$

Similarly, a product of two matrices is a block matrix, e.g.

$$\boldsymbol{A}\otimes\boldsymbol{B} = \begin{bmatrix} A_{11}\boldsymbol{B} & A_{12}\boldsymbol{B} \\ A_{21}\boldsymbol{B} & A_{22}\boldsymbol{B} \end{bmatrix}$$

Combining all of our vectors $\boldsymbol{x}^i$ into a vector-of-vectors $\boldsymbol{X}$,

$$\boldsymbol{X} = (x_1^1, x_2^1, \ldots, x_1^N, x_2^N)^{\mathrm{T}}$$

we can rewrite our ODE to include all *N* cells. Our final ODE is

$$\frac{d\boldsymbol{X}}{dt} = (\boldsymbol{I_N} \otimes \boldsymbol{K} + \boldsymbol{M} \otimes \boldsymbol{B})\boldsymbol{X} = \boldsymbol{J}\boldsymbol{X} \tag{A1.8}$$

where $\boldsymbol{M}$ represents an $N \times N$ "connectivity matrix" that describes which cells are contacting one another. A connectivity matrix can be easily demonstrated using a 4-membered ring of cells, as depicted in Fig. 3 of the main text.

The $\boldsymbol{J}$ term of Equation A1.6 is the Jacobian matrix corresponding to our homogenous steady-state. The eigenvalues of this Jacobian will tell us if the system is stable or unstable. If all eigenvalues are negative, the system will tend back towards the homogeneous steady-state following a minor perturbation of any input. If any eigenvalue is positive, the system is unstable and will deviate away from the UNESS solution following any fluctuation.

Othmer and Scriven (1971) vastly simplified the process of finding all $n \times N$ (n being the number of chemical species) eigenvalues of Eq. 8 by separating the effect that network structure (connectivity) has on the Jacobian. Our strategy is to first determine the eigenvectors and eigenvalues of the connectivity matrix $\boldsymbol{M}$, which represent the "structural modes" of the network and are somewhat analogous to the normal modes of classical vibration. From there, we can independently determine the stability of each structural mode.

The following was based on a description of the method given by Plahte (2001). To begin, let us assume $\boldsymbol{M}$ can be diagonalized by a matrix $\boldsymbol{U}$ containing the eigenvectors $\boldsymbol{U}^{(k)}$ of $\boldsymbol{M}$:

$$\boldsymbol{U}^{-1}\boldsymbol{M}\boldsymbol{U} = \boldsymbol{D} = \begin{bmatrix} q_1 & 0 & 0 \\ 0 & \ddots & 0 \\ 0 & 0 & q_N \end{bmatrix}$$

where $\boldsymbol{D}$ is an $N \times N$ diagonal matrix containing the eigenvalues of $\boldsymbol{M}$, q_k. Define $\boldsymbol{T} = \boldsymbol{U}\otimes\boldsymbol{I_n}$, and define

$$\boldsymbol{L} = \boldsymbol{T}^{-1}\boldsymbol{J}\boldsymbol{T} = (\boldsymbol{U}^{-1}\otimes\boldsymbol{I_n})(\boldsymbol{I_N}\otimes\boldsymbol{K} + \boldsymbol{M}\otimes\boldsymbol{B})(\boldsymbol{U}\otimes\boldsymbol{I_n})$$

In essence, $\boldsymbol{L}$ is our Jacobian ($\boldsymbol{J}$) for $\boldsymbol{X}$ that has been transformed to be in the orthonormal basis of our structural eigenvectors $\boldsymbol{U}^{(k)}$. Using an identity of our previously defined tensor product,

$$(\boldsymbol{A}\otimes\boldsymbol{B})(\boldsymbol{C}\otimes\boldsymbol{D}) = (\boldsymbol{A}\boldsymbol{C})\otimes(\boldsymbol{B}\boldsymbol{D})$$

we can simplify our expression for $\boldsymbol{L}$.

$$\boldsymbol{L} = [(\boldsymbol{U}^{-1}\boldsymbol{I_N})\otimes(\boldsymbol{I_n}\boldsymbol{K}) + (\boldsymbol{U}^{-1}\boldsymbol{M})\otimes(\boldsymbol{I_n}\boldsymbol{B})](\boldsymbol{U}\otimes\boldsymbol{I_n})$$

$$\boldsymbol{L} = (\boldsymbol{U}^{-1}\boldsymbol{I_N}\boldsymbol{U})\otimes(\boldsymbol{I_n}\boldsymbol{K}\boldsymbol{I_n}) + (\boldsymbol{U}^{-1}\boldsymbol{M}\boldsymbol{U})\otimes(\boldsymbol{I_n}\boldsymbol{B}\boldsymbol{I_n})$$

$$\boldsymbol{L} = \boldsymbol{I_N}\otimes\boldsymbol{K} + \boldsymbol{D}\otimes\boldsymbol{B}$$

$\boldsymbol{L}$ is now a $N \times N$ block diagonal where each block k contains an $n \times n$ matrix (in our case 2×2) corresponding to the state of a cell in the structural mode k. Each block $\boldsymbol{H}^{(k)}$ in $\boldsymbol{L}$ is

$$\boldsymbol{H}^{(k)} = \boldsymbol{K} + q_k\boldsymbol{B}$$

where q_k is the eigenvalue for the corresponding structural mode and $k = 1,2,...,N$. The characteristic equation determining the eigenvalues of L is given by

$$\det(\boldsymbol{L} - \lambda\boldsymbol{I}) = 0$$

which can be rewritten in terms of the block components.

$$\det\left(\mathrm{diag}\left(\boldsymbol{H}^{(k)} - \lambda\boldsymbol{I_n}\right)\right) = \det\left(\mathrm{diag}(\boldsymbol{K} + q_k\boldsymbol{B} - \lambda\boldsymbol{I_n})\right) = 0 \qquad \text{(A1.9)}$$

A property of the block diagonal matrix is that the overall determinant is a product of its blocks:

$$\det(\boldsymbol{A}) = \det(\boldsymbol{A_1}) \times \ldots \times \det(\boldsymbol{A_n})$$

Thus, our overall characteristic equation for the eigenvalues of our Jacobian becomes

$$\det\left(\boldsymbol{K} + q_k\boldsymbol{B} - \lambda_{k\mu}\boldsymbol{I_n}\right) = 0 \qquad \text{(A1.10)}$$

where □ = 1 or 2 (species VEGFR2 and Delta). This much simpler determinant can be evaluated independently for every value of q_k to predict the stability of the homogeneous steady-state based on the signs of the eigenvalues $\lambda_{k\mu}$. In the case of our VEGFR2-Delta-Notch system, the characteristic determinant for every q_k can be expressed by going back to our definitions from Eqs. A1.5 and A1.6. The eigenvalues are found using the determinant

$$\begin{vmatrix} \frac{\partial r_R(R_i)}{\partial R_i} - \lambda_{k1} & q_k \frac{\partial f_R(\langle D_i \rangle)}{\partial \langle D_i \rangle} \\ \frac{\partial f_D(R_i)}{\partial R_i} & \frac{\partial r_D(D_i)}{\partial D_i} - \lambda_{k2} \end{vmatrix} = 0 \qquad \text{(A1.11)}$$

This determinant leads to a quadratic equation for the eigenvalues, solved using the quadratic formula

$$\lambda_{\pm} = -1/2 \left[\left(\frac{\partial r_R(R_i)}{\partial R_i} + \frac{\partial r_D(D_i)}{\partial D_i} \right) \pm \sqrt{\left(\frac{\partial r_R(R_i)}{\partial R_i} + \frac{\partial r_D(D_i)}{\partial D_i} \right)^2 - 4 \left(\frac{\partial r_R(R_i)}{\partial R_i} \frac{\partial r_D(D_i)}{\partial D_i} - q_k \frac{\partial f_R(\langle D_i \rangle)}{\partial \langle D_i \rangle} \frac{\partial f_D(R_i)}{\partial R_i} \right)} \right]$$

The homogeneous steady-state is only unstable if one or more of the eigenvalues is positive. To illustrate when we will get a positive real eigenvalue, let us restate the

equation using simple variables and assume that we shall use the "minus" from the $\pm$ operator.

$$\lambda_{-} = {}^{-1}/_{2}\left[b - \sqrt{b^2 - 4(a-c)}\right]$$

If $a < c$, the $a - c$ term is negative and the argument of the radical becomes larger than b^2. Subtracting the square root of that larger-than-b^2 term means that $b - \sqrt{b^2 - 4(a-c)}$ is negative and real. Multiplying this by ${}^{-1}/_{2}$ yields a positive real number. From this, we can gather that we will only get a positive real eigenvalue if the following condition is met:

$$-q_k \frac{\partial \dot{R}_i}{\partial \langle D_i \rangle}\bigg|_{SS} \frac{\partial \dot{D}_i}{\partial R_i}\bigg|_{SS} - \frac{\partial \dot{R}_i}{\partial R_i}\bigg| \frac{\partial \dot{D}_i}{\partial D_i}\bigg| > 0 \qquad \text{(A1.12)}$$

This is the general form of the criteria for instability for Delta-Notch lateral inhibition. The same approach outlined in this section can be used to calculate the stability criteria for any problem of juxtacrine signaling in a regular lattice of cells, and we shall use it to calculate the stability criteria for each hypothetical GRN shown in Fig. 1 *B* of the main text.

APPENDIX A2

STABILITY ANALYSIS FOR THE CLASSICAL GRN

The classical GRN of tip-stalk selection (Fig. 1 B *i*) is governed by two ODEs and two pseudo-steady-state rate laws for signaling.

$$\frac{dR_i}{dt} = \beta_R \frac{(k_{RNA})^{n_R}}{(k_{RNA})^{n_R} + (N_{Ai})^{n_R}} - \gamma_R R_i \tag{A2.1}$$

$$\frac{dD_i}{dt} = \beta_D \frac{(R_A)^{n_D}}{(k_{DRA})^{n_D} + (R_A)^{n_D}} - \gamma_D D_i \tag{A2.2}$$

$$R_A = \frac{V_i R_i}{k_V} \tag{A2.3}$$

$$N_{Ai} = \frac{N_i}{n k_N \gamma_{NA}} \sum D_{j \neq i} = K_N N_i \langle D \rangle_i \tag{A2.4}$$

To calculate the stability of the endothelium about the homogeneous steady-state, we first need to define the steady-state homogeneous expression of each species.

$$R_{ss} = \frac{\beta_R}{\gamma_R} \frac{(k_{RNA})^{n_R}}{(k_{RNA})^{n_R} + (k_N D_{ss} N_i)^{n_R}} \tag{A2.5}$$

$$D_{ss} = \frac{\beta_D}{\gamma_D} \frac{\left(\frac{V R_{ss}}{k_V}\right)^{n_D}}{(k_{DRA})^{n_D} + \left(\frac{V R_{ss}}{k_V}\right)^{n_D}} \tag{A2.6}$$

We can perform the series expansion about this homogeneous steady-state by taking the relevant partial derivatives and evaluating them at the steady-state conditions. For the equation governing Delta expression,

$$\frac{\partial \dot{D}_i}{\partial D_i} = -\gamma_D \tag{A2.7}$$

$$\left.\frac{\partial \dot{D}_i}{\partial R_i}\right|_{ss} = \beta_D n_D \frac{(k_{DRA})^{n_D}}{R_{ss}} \frac{\left(\frac{VR_{ss}}{k_V}\right)^{n_D}}{\left((k_{DRA})^{n_D} + \left(\frac{VR_{ss}}{k_V}\right)^{n_D}\right)^2} = \gamma_D n_D \frac{D_{ss}}{R_{ss}} \frac{(k_{DRA})^{n_D}}{(k_{DRA})^{n_D} + \left(\frac{VR_{ss}}{k_V}\right)^{n_D}} \tag{A2.8}$$

For convenience, we define a variable g_D that contains the remaining nonlinear term, which can range numerically from 0 to 1:

$$g_D = \frac{(k_{DRA})^{n_D}}{(k_{DRA})^{n_D} + \left(\frac{VR_{ss}}{k_V}\right)^{n_D}} \tag{A2.9}$$

$$\left.\frac{\partial \dot{D}_i}{\partial R_i}\right|_{ss} = \gamma_D n_D \frac{D_{ss}}{R_{ss}} g_D \tag{A2.10}$$

We can perform the same steps on the equation for VEGFR2 expression,

$$\frac{\partial \dot{R}_i}{\partial R_i} = -\gamma_R \tag{A2.11}$$

$$\left.\frac{\partial \dot{R}_i}{\partial \langle D_i \rangle}\right|_{ss} = -\frac{\beta_R n_R}{D_{ss}} (k_{RNA})^{n_R} \frac{(k_N D_{ss} N_i)^{n_R}}{((k_{RNA})^{n_R} + (K_N D_{ss} N_i)^{n_R})^2} = -\gamma_R n_R \frac{R_{ss}}{D_{ss}} \frac{(k_N D_{ss} N_i)^{n_R}}{(k_{RNA})^{n_R} + (K_N D_{ss} N_i)^{n_R}} \tag{A2.12}$$

$$g_R = \frac{(K_N D_{ss} N_i)^{n_R}}{(k_{RNA})^{n_R} + (K_N D_{ss} N_i)^{n_R}} \tag{A2.13}$$

$$\left.\frac{\partial \dot{R}_i}{\partial \langle D_i \rangle}\right|_{ss} = -\gamma_R n_R \frac{R_{ss}}{D_{ss}} g_R \tag{A2.14}$$

Our matrices from Equation A1.5 and A1.6 become

$$\boldsymbol{K} = \begin{bmatrix} -\gamma_R & 0 \\ \gamma_D n_D \dfrac{D_{ss}}{R_{ss}} g_D & -\gamma_D \end{bmatrix} \tag{A2.15}$$

$$\boldsymbol{B} = \begin{bmatrix} 0 & -\dfrac{\gamma_R R_s n}{D_s} g_0 \\ 0 & 0 \end{bmatrix} \tag{A2.16}$$

We can evaluate the characteristic equation for stability (Eq. A1.10) to find our most positive eigenvalue, or Maximal Lyapunov Exponent (MLE).

$$\lambda_{\pm} = {}^{-1}/_{2} \Big[(-\gamma_R - \gamma_D) \pm \sqrt{(-\gamma_R - \gamma_D)^2 - 4(\gamma_R \gamma_D + q_k \gamma_R \gamma_D n_R n_D g_R g_D)} \Big] \tag{A2.17}$$

The eigenvalue has a positive real component when the discriminant of the Jacobian is negative. As such, the criteria for instability under the classical GRN is

$$\gamma_R \gamma_D + q_k \gamma_R \gamma_D n_R n_D g_R g_D < 0 \tag{A2.18}$$

Or,

$$-q_k n_R n_D g_R g_D - 1 > 0 \tag{A2.19}$$

where the left-hand side of Equation A2.19 is equal in sign and proportional to the MLE. The terms g_R and g_D cannot be found analytically for most Hill coefficients; the steady-states of VEGFR2 and Delta must be evaluated numerically to determine the homogeneous stability of the GRN. A null-cline plot (such as in Figure 5) can aide in visualizing the solution. Including basal expression from Eqs. 10 and 11 from the main text results in a similar criteria for instability:

$$-q_k n_R n_D g_R g_D \left(1 - {}^{\alpha_R}/_{\gamma_R R_{ss}}\right)\left(1 - {}^{\alpha_D}/_{\gamma_D D_{ss}}\right) - 1 \geq 0 \tag{A2.20}$$

APPENDIX A3

STABILITY ANALYSIS OF 'REGULATED NOTCH'

This derivation for the stability criterion for the 'Regulated Notch' (Fig 1 *B ii*) differs from the classical case because it involves three species with dynamic regulation. The overarching method is very similar, however. The three ODEs that model the 'Regulated Notch' GRN are as follow:

$$\frac{dN_i}{dt} = \beta_N \frac{(R_A)^{n_N}}{(k_{NRA})^{n_N} + (R_A)^{n_N}} - \gamma_N N_i \tag{A3.1}$$

$$\frac{dR_i}{dt} = \beta_R \frac{(k_{RNA})^{n_R}}{(k_{RNA})^{n_R} + (N_{Ai})^{n_R}} - \gamma_R R_i \tag{A3.2}$$

$$\frac{dD_i}{dt} = \beta_D \frac{(R_A)^{n_D}}{(k_{DRA})^{n_D} + (R_A)^{n_D}} - \gamma_D D_i \tag{A3.3}$$

The signaling kinetics (Eqs. A2.3 and A2.4) are unchanged. As in the previous example, we first find define the homogeneous steady-state of each species.

$$N_{ss} = \frac{\beta_N}{\gamma_N} \frac{\left(\frac{VR_{ss}}{k_V}\right)^{n_N}}{(k_{NRA})^{n_N} + \left(\frac{VR_{ss}}{k_V}\right)^{n_N}} \tag{A3.4}$$

$$R_{ss} = \frac{\beta_R}{\gamma_R} \frac{(k_{RNA})^{n_R}}{(k_{RNA})^{n_R} + (K_N D_{ss} N_{ss})^{n_R}} \tag{A3.5}$$

$$D_{ss} = \frac{\beta_D}{\gamma_D} \frac{\left(\frac{VR_{ss}}{k_V}\right)^{n_D}}{(k_{DRA})^{n_D} + \left(\frac{VR_{ss}}{k_V}\right)^{n_D}} \tag{A3.6}$$

Now, we can linearize each species with respect to its input(s) about the homogeneous steady-state:

$$\left.\frac{d\dot{N}_i}{dR_i}\right|_{ss} = \beta_N n_N \frac{(k_{RAN})^{n_N}}{R_{ss}} \frac{\left(\frac{VR_{ss}}{k_V}\right)^{n_N}}{\left((k_{NRA})^{n_1} + \left(\frac{VR_{ss}}{k_V}\right)^{n_1}\right)^2} \tag{A3.7}$$

$$\left.\frac{d\dot{N}_i}{dR_i}\right|_{ss} = \gamma_N \frac{N_{ss}}{R_{ss}} n_N \frac{(k_{NRA})^{n_N}}{(k_{NRA})^{n_N} + \left(\frac{VR_{ss}}{k_V}\right)^{n_N}} \tag{A3.8}$$

$$g_N = \frac{(k_{NRA})^{n_N}}{(k_{NRA})^{n_N} + \left(\frac{VR_{ss}}{k_V}\right)^{n_N}} \tag{A3.9}$$

$$\left.\frac{d\dot{N}_i}{dR_i}\right|_{ss} = \gamma_N n_N g_N \frac{N_{ss}}{R_{ss}} \tag{A3.10}$$

The equation for VEGFR2 now has to independent inputs, N_i and $\langle D \rangle_i$,

$$\left.\frac{d\dot{R}_i}{d\langle D \rangle_i}\right|_{ss} = -\beta_R n_R \frac{(k_{RNA})^{n_R}}{D_{ss}} \frac{(K_N D_{ss} N_{ss})^{n_R}}{((k_{RNA})^{n_R} + (K_N D_{ss} N_{ss})^{n_R})^2} \tag{A3.11}$$

$$\left.\frac{d\dot{R}_i}{d\langle D \rangle_i}\right|_{ss} = -\gamma_R \frac{R_{ss}}{D_{ss}} n_R \frac{(K_N D_{ss} N_{ss})^{n_R}}{(k_{RNA})^{n_R} + (K_N D_{ss} N_{ss})^{n_R}} \tag{A3.12}$$

$$g_R = \frac{(K_N D_{ss} N_{ss})^{n_R}}{(k_{RNA})^{n_R} + (K_N D_{ss} N_{ss})^{n_R}} \tag{A3.13}$$

$$\left.\frac{d\dot{R}_i}{d\langle D \rangle_i}\right|_{ss} = -\gamma_R \frac{R_{ss}}{D_{ss}} n_R g_R \tag{A3.14}$$

$$\left.\frac{d\dot{R}_i}{dN_i}\right|_{ss} = -\beta_R n_R \frac{(k_{RNA})^{n_R}}{N_{ss}} \frac{(k_N D_{ss} N_{ss})^{n_R}}{((k_{RNA})^{n_R} + (K_N D_{ss} N_{ss})^{n_R})^2} \tag{A3.15}$$

$$\left.\frac{d\dot{R}_i}{dN_i}\right|_{ss} = -\gamma_R \frac{R_{ss}}{N_{ss}} n_R g_R \tag{A3.16}$$

The result for Delta expression is the same as in the classical case case (Eq. A2.10):

$$\left.\frac{d\dot{D}_i}{dR_i}\right|_{ss} = \gamma_D \frac{D_{ss}}{R_{ss}} n_D g_D \tag{A3.17}$$

Our 3 x 3 matrices $\boldsymbol{K}$ and $\boldsymbol{B}$ incorporate the linearized result of each equation,

$$\boldsymbol{K} = \begin{bmatrix} \frac{dF}{dN_i} & \frac{dF}{dR_i} & \frac{dF}{dD_i} \\ \frac{dG}{dN_i} & \frac{dG}{dR_i} & \frac{dG}{dD_i} \\ \frac{dH}{dN_i} & \frac{dH}{dR_i} & \frac{dH}{dD_i} \end{bmatrix} = \begin{bmatrix} -\gamma_N & \gamma_N n_N g_N \frac{N_{ss}}{R_{ss}} & 0 \\ -\gamma_R \frac{R_{ss}}{N_{ss}} n_R g_R & -\gamma_R & 0 \\ 0 & \gamma_D \frac{D_{ss}}{R_{ss}} n_D g_D & -\gamma_D \end{bmatrix} \tag{A3.18}$$

$$\boldsymbol{B} = \begin{bmatrix} \frac{dF}{d\langle N\rangle_i} & \frac{dF}{d\langle R\rangle_i} & \frac{dF}{d\langle D\rangle_i} \\ \frac{dG}{d\langle N\rangle_i} & \frac{dG}{d\langle R\rangle_i} & \frac{dG}{d\langle D\rangle_i} \\ \frac{dH}{d\langle N\rangle_i} & \frac{dH}{d\langle R\rangle_i} & \frac{dH}{d\langle D\rangle_i} \end{bmatrix} = \begin{bmatrix} 0 & 0 & 0 \\ 0 & 0 & -\gamma_R \frac{R_{ss}}{D_{ss}} n_R g_R \\ 0 & 0 & 0 \end{bmatrix} \tag{A3.19}$$

The characteristic equation (Eq. A1.10) can be used to generate a polynomial for the eigenvalues of the homogeneous steady state. Because or matrix is 3 x 3, the quadratic formula cannot be used to find all of our eigenvalues, but we can find any switch-like behavior in our system by ignoring the higher-order terms of our characteristic polynomial (not shown). It can be shown that that an eigenvalue passes through the origin from negative to positive when

$$\gamma_R \gamma_D + n_N n_R \gamma_N \gamma_R g_N g_R + q_k n_R n_D \gamma_R \gamma_D g_R g_D < 0 \tag{A3.20}$$

Our MLE is therefore equal in sign and proportional to

$$-q_k n_R n_D g_R g_D - n_N n_R \frac{\gamma_N}{\gamma_D} g_N g_R - 1 < 0 \tag{A3.21}$$

when the system is near the homogeneous steady-state and only moderately stable or unstable.

APPENDIX A4

STABILITY ANALYSIS FOR THE 'DELTA FEED-FORWARD' GRN

This formulation for the "Delta feed-forward" GRN (Fig. 1 *B iii*) makes both VEGFR2 and Delta expression governed by Notch signaling, in line with observations by Caolo, *et al* [23].

$$\frac{dD_i}{dt} = \beta_D \frac{(k_{DNA})^{n_D}}{(k_{DNA})^{n_D} + (N_{Ai})^{n_D}} - \gamma_D D_i \tag{A4.1}$$

Equation 1 from the main text still applies. In addition, VEGFR2 activation modulates the level of Notch signaling.

$$N_{Ai} = \frac{N_i}{nk_N\gamma_{NA}} \sum D_{j\neq i} \left(\frac{(R_{Ai})^{n_A}}{(k_{NRA})^{n_A} + (R_{Ai})^{n_A}} \right) \tag{A4.2}$$

The steady state value of VEGFR2 expression, Delta expression, and Notch activation are given by

$$R_{ss} = \frac{\beta_R}{\gamma_R} \frac{(k_{RNA})^{n_R}}{(k_{RNA})^{n_R} + (N_{Ass})^{n_R}} \tag{A4.3}$$

$$D_{ss} = \frac{\beta_D}{\gamma_D} \frac{(N_{Ass})^{n_D}}{(k_{DNA})^{n_D} + (N_{Ass})^{n_D}} \tag{A4.4}$$

$$N_{Ass} = K_N N_i D_{ss} \frac{\left(\frac{VR_{ss}}{k_V}\right)^{n_A}}{(k_{NRA})^{n_A} + \left(\frac{VR_{ss}}{k_V}\right)^{n_A}} \tag{A4.5}$$

Because both VEGFR2 and Delta expression are now dependent on both VEGFR2 and Notch signaling, we need to take corresponding partial derivatives for each species. First, we find the change in VEGFR2 with respect to itself.

$$\left.\frac{d\dot{R}_i}{dR_i}\right|_{ss} = -\gamma_R - \frac{\beta_R n_R}{N_{Ass}} \frac{(k_{RNA})^{n_R}(N_{Ai})^{n_R}}{((k_{RNA})^{n_R} + (N_{Ai})^{n_R})^2} \times \left.\frac{dN_{Ai}}{dR_i}\right|_{ss} \tag{A4.6}$$

$$g_R = \frac{(N_{Ai})^{n_R}}{(k_{RNA})^{n_R} + (N_{Ai})^{n_R}} \tag{A4.7}$$

$$\left.\frac{d\dot{R}_i}{dR_i}\right|_{ss} = -\gamma_R - \gamma_R \frac{n_R R_{ss}}{N_{Ass}} g_R \times \left.\frac{dN_{Ai}}{dR_i}\right|_{ss} \tag{A4.8}$$

$$\left.\frac{dN_{Ai}}{dR_i}\right|_{ss} = \frac{K_N N_i D_{ss} n_A}{R_{ss}} \frac{(k_{NRA})^{n_A}\left(\frac{VR_{ss}}{k_V}\right)^{n_A}}{\left((k_{NRA})^{n_A} + \left(\frac{VR_{ss}}{k_V}\right)^{n_A}\right)^2} \tag{A4.7}$$

$$g_A = \frac{(k_{NRA})^{n_A}}{(k_{NRA})^{n_A} + \left(\frac{VR_{ss}}{k_V}\right)^{n_A}} \tag{A4.8}$$

$$\left.\frac{dN_{Ai}}{dR_i}\right|_{ss} = \frac{n_A N_{Ass} g_A}{R_{ss}} \tag{A4.9}$$

$$\left.\frac{d\dot{R}_i}{dR_i}\right|_{ss} = -\gamma_R - \gamma_R \frac{n_R R_{ss}}{N_{Ass}} g_R \times \frac{n_A N_{Ass}}{R_{ss}} g_A \tag{A4.10}$$

$$\left.\frac{d\dot{R}_i}{dR_i}\right|_{ss} = -\gamma_R(1 + n_R g_R n_A g_A) \tag{A4.11}$$

The response of VEGFR2 expression with respect to neighboring Delta is unchanged from the classical case (Eq. A2.14).

$$\left.\frac{d\dot{R}_i}{d\langle D\rangle_i}\right|_{ss} = \gamma_R \frac{R_{ss}}{D_{ss}} n_R g_R \tag{A4.14}$$

Next, we find the change in Delta expression with respect to VEGFR2.

$$\left.\frac{d\dot{D}_i}{dR_i}\right|_{ss} = \left.\frac{d\dot{D}_i}{dN_{Ai}}\right|_{ss} \times \left.\frac{dN_{Ai}}{dR_i}\right|_{ss}$$
$$= \frac{\beta_D n_D}{N_{Ass}} \frac{(k_{DNA})^{n_D}(N_{Ass})^{n_D}}{((k_{DNA})^{n_D} + (N_{Ass})^{n_D})^2} \times \left.\frac{dN_{Ai}}{dR_i}\right|_{ss} \quad \text{(A4.15)}$$

$$g_D = \frac{(k_{DNA})^{n_D}}{(k_{DNA})^{n_D} + (K_N D_{ss} N_{ss})^{n_D}} \quad \text{(A4.16)}$$

$$\left.\frac{d\dot{D}_i}{dR_i}\right|_{ss} = \frac{\gamma_D n_D D_{ss} g_D}{N_{Ass}} \left.\frac{dN_{Ai}}{dR_i}\right|_{ss} \quad \text{(A4.17)}$$

$$\left.\frac{d\dot{D}_i}{dR_i}\right|_{ss} = \gamma_D n_D g_D n_A g_A \frac{D_{ss}}{R_{ss}} \quad \text{(A4.18)}$$

Next, we take the derivative of Delta with respect to itself

$$\left.\frac{d\dot{D}_i}{dD_i}\right|_{ss} = -\gamma_D \quad \text{(A4.19)}$$

The only remaining step is the partial derivative of Delta with respect to neighboring

$$\left.\frac{d\dot{D}_i}{d\langle D\rangle_i}\right|_{ss} = \frac{\beta_D n_D}{N_{Ass}} \frac{(k_{DNA})^{n_D}(N_{Ass})^{n_D}}{((k_{DNA})^{n_D} + (N_{Ass})^{n_D})^2} \left.\frac{dN_{Ai}}{d\langle D\rangle_i}\right|_{ss} \quad \text{(A4.20)}$$

$$\left.\frac{dN_{Ai}}{d\langle D\rangle_i}\right|_{ss} = K_N N_i \frac{\left(\frac{VR_{ss}}{k_V}\right)^{n_A}}{(k_{NRA})^{n_A} + \left(\frac{VR_{ss}}{k_V}\right)^{n_A}} = \frac{N_{Ass}}{D_{ss}} \quad \text{(A4.21)}$$

$$\left.\frac{d\dot{D}_i}{d\langle D\rangle_i}\right|_{ss} = \gamma_D n_D g_D \frac{D_{ss}}{N_{Ass}} \frac{N_{Ass}}{D_{ss}} \quad \text{(A4.22)}$$

$$\left.\frac{d\dot{D}_i}{d\langle D\rangle_i}\right|_{ss} = \gamma_D n_D g_D \quad \text{(A4.21)}$$

Our matrices $\boldsymbol{K}$ and $\boldsymbol{B}$ become

$$\boldsymbol{K} = \begin{bmatrix} -\gamma_R(1 + n_R g_R n_A g_A) & 0 \\ \gamma_D n_D g_D n_A g_A \dfrac{D_{ss}}{R_{ss}} & -\gamma_D \end{bmatrix} \tag{A4.22}$$

$$\boldsymbol{B} = \begin{bmatrix} 0 & -\gamma_R n_R g_R \dfrac{R_{ss}}{D_{ss}} \\ 0 & \gamma_D n_D g_D \end{bmatrix} \tag{A4.23}$$

The governing equation for our system eigenvalues is

$$\begin{vmatrix} -\gamma_R(1 + n_R g_R n_A g_A) - \lambda_{k1} & -q_k \gamma_R n_R g_R \dfrac{R_{ss}}{D_{ss}} \\ \gamma_D n_D g_D n_A g_A \dfrac{D_{ss}}{R_{ss}} & q_k \gamma_D (n_D g_D - 1) - \lambda_{k2} \end{vmatrix} = 0 \tag{A4.24}$$

The resulting quadratic equation for our system eigenvalues is

$$\lambda^2 + (g_A g_R \gamma_R n_A n_R - {\gamma_D}^2 n_D q_k + \gamma_D + \gamma_R)\lambda + (-g_D n_D q_k + g_A g_R n_R n_A + 1) = 0 \tag{A4.24}$$

Using the quadratic formula, we can show that there is a positive eigenvalue only when

$$q_k n_D g_D - n_R n_A g_A g_R - 1 > 0 \tag{A4.25}$$

The system is stable or will undergo uniform differentiation. In this system q_k has to be positive for any chance of instability, and this does not correspond to patterning (the bifurcation of neighboring cell phenotypes) like in the other stability criteria. By our interpretation (i.e. the assumed kinetic rate laws), the "Delta Feed-Forward" GRN is incapable of pattern formation.

APPENDIX A5

STABILITY ANALYSIS FOR THE 'VEGFR1 EXPRESSION' GRN

This analysis determines the stability criterion for the "VEGFR1 expression" GRN (Fig. 1 *B iv*), wherein Notch signaling up-regulates the expression of a nonproductive receptor for VEGF. The system is now represented by the following three ODEs and two steady-state signaling rate laws

$$\frac{dR_i}{dt} = \beta_R \frac{(k_{RNA})^{n_R}}{(k_{RNA})^{n_R} + (N_{Ai})^{n_R}} - \gamma_R R_i \tag{A5.1}$$

$$\frac{dD_i}{dt} = \beta_D \frac{(R_{Ai})^{n_R}}{(k_{DRA})^{n_R} + (R_{Ai})^{n_R}} - \gamma_D D_i \tag{A5.2}$$

$$\frac{dS_i}{dt} = \beta_S \frac{(N_{Ai})^{n_S}}{(k_{SNA})^{n_S} + (N_{Ai})^{n_S}} - \gamma_S S_i + \frac{K_s}{\nu} \sum \left(S_{j \neq i} - S_i\right) \tag{A5.3}$$

$$N_{Ai} = K_N N_i \langle D \rangle_i \tag{A5.4}$$

$$R_{Ai} = \frac{V_i}{k_v(1 + k_s S_i)} R_i \tag{A5.5}$$

The steady-state values of each species are

$$R_{ss} = \frac{\beta_R}{\gamma_R} \frac{(k_{RNA})^{n_R}}{(k_{RNA})^{n_R} + (K_N N_i D_{ss})^{n_R}} \tag{A5.6}$$

$$D_{ss} = \frac{\beta_D}{\gamma_D} \frac{\left(\frac{V_i}{k_v(1 + k_s S_{ss})} R_{ss}\right)^{n_R}}{(k_{DRA})^{n_R} + \left(\frac{V_i}{k_v(1 + k_s S_{ss})} R_{ss}\right)^{n_R}} \tag{A5.7}$$

$$S_{ss} = \frac{\beta_S}{\gamma_S} \frac{(N_{Ai})^{n_S}}{(k_{SNA})^{n_S} + (N_{Ai})^{n_S}} \tag{A5.8}$$

Notice there is no influence of the flux in the steady-state values of VEGFR1. This is because there is no net intercellular flux in a homogeneous steady-state. We proceed to find the partial derivatives of each ODE. The partial derivative of $\dot{R}_i$ and $\dot{D}_i$ are the

same as in the classical case, with the exception that $\dot{D}_i$ now has a derivative with respect to S_i. This is the same as the derivative with respect to R_i except with a substation for the signaling derivative.

$$\left.\frac{dR_{Ai}}{dR_i}\right|_{ss} = \frac{k_s}{1 + k_s S_{ss}} \tag{A5.9}$$

$$\left.\frac{dR_{Ai}}{dS_i}\right|_{ss} = -k_s \frac{V_i R_{ss}}{k_v (1 + k_s S_{ss})^2} \tag{A5.10}$$

$$\left.\frac{d\dot{D}_i}{dR_i}\right|_{ss} = \gamma_D \frac{D_{ss}}{R_{ss}} n_D g_D \tag{A5.11}$$

$$\left.\frac{d\dot{D}_i}{dS_i}\right|_{ss} = -\frac{k_s}{1 + k_s S_{ss}} \gamma_D D_{ss} n_D g_D \tag{A5.12}$$

The partial derivatives of $\dot{S}_i$ also need to be calculated.

$$\left.\frac{d\dot{S}_i}{d\langle D\rangle_i}\right|_{ss} = \frac{\beta_S n_S}{D_{ss}} \frac{(k_{SNA})^{n_S} (K_N N_i D_{ss})^{n_S}}{((k_{SNA})^{n_S} + (K_N N_i D_{ss})^{n_S})^2} \tag{A5.13}$$

$$\left.\frac{d\dot{S}_i}{d\langle D\rangle_i}\right|_{ss} = \gamma_S n_S \frac{S_{ss}}{D_{ss}} \frac{(k_{SNA})^{n_S}}{(k_{SNA})^{n_S} + (K_N N_i D_{ss})^{n_S}} \tag{A5.14}$$

$$g_S = \frac{(k_{SNA})^{n_S}}{(k_{SNA})^{n_S} + (K_N N_i D_{ss})^{n_S}} \tag{A5.15}$$

$$\left.\frac{d\dot{S}_i}{d\langle D\rangle_i}\right|_{ss} = \gamma_S n_S \frac{S_{ss}}{D_{ss}} g_S \tag{A5.16}$$

$$\left.\frac{d\dot{S}_i}{d\langle S\rangle_i}\right|_{ss} = K_s \tag{A5.17}$$

$$\left.\frac{d\dot{S}_i}{dS_i}\right|_{ss} = -\gamma_S - K_s \tag{A5.18}$$

Our 3 $\times$ 3 matrices $\boldsymbol{K}$ and $\boldsymbol{B}$ become

$$\boldsymbol{K} = \begin{bmatrix} -\gamma_R & 0 & 0 \\ \gamma_D \frac{D_{ss}}{R_{ss}} n_D g_D & -\gamma_D & -\frac{k_s}{1+k_s S_{ss}} \gamma_D D_{ss} n_D g_D \\ 0 & 0 & -\gamma_S - K_s \end{bmatrix} \tag{A5.19}$$

$$\boldsymbol{B} = \begin{bmatrix} 0 & -\gamma_R \frac{R_{ss}}{D_{ss}} n_R g_R & 0 \\ 0 & 0 & 0 \\ 0 & \gamma_S n_S \frac{S_{ss}}{D_{ss}} g_S & K_s \end{bmatrix} \tag{A5.20}$$

Like in the case of 'Regulated Notch' we are left with a third-order polynomial to determine our overall eigenvalues. Again, we will make the assumption that the system has marginal stability at some point with respect to VEGF, so we only look for small positive eigenvalues. It can be shown that an eigenvalue is positive when the following condition is met:

$$-q_k n_R n_D g_R g_D - \frac{q_k}{\left(1 + (1-q_k)\frac{K_s}{\gamma_S}\right)} n_D n_S g_D g_S \frac{k_s S_{ss}}{1 + k_s S_{ss}} - 1 \geq 0 \tag{A5.21}$$

Compared to the other stability criteria of Table 1, the homogeneous stability of this GRN has a more complicated dependence on the structural eigenvalue q_k. In the absence of diffusion ($K_s = 0$) the expression of VEGFR1 in response to Notch signaling clearly reinforces lateral inhibition and contributes to the instability of the HSS. As K_s is increased, this effect is reduced. It should be noted that largest negative eigenvalues of q_k are still the most unstable in this system, implying that a system with diffusible VEGFR1 still tends to form close-packed patterns.

REFERENCES

[1] Kim, K., B. Li, … N. Gillett. 1993. Inhibition of vascular endothelial growth factor-induced angiogenesis suppresses tumour growth *in vivo*. *Nature*. 362.

[2] Zheng, Y., J. Chen, ..., A.D. Stroock. 2012. *In vitro* microvessels for the study of angiogenesis and thrombosis. *Proc. Natl. Acad. Sci. U. S. A.* 109: 9342–7.

[3] Folkman, J. 1982. Angiogenesis: Initiation and Control. *Ann. N. Y. Acad. Sci.* 7: 212–227.

[4] Gerhardt, H., M. Golding, … C. Betsholtz. 2003. VEGF guides angiogenic sprouting utilizing endothelial tip cell filopodia. *J. Cell Biol.* 161: 1163–77.

[5] Hellström, M., L.-K. Phng, … C. Betsholtz. 2007. Dll4 signalling through Notch1 regulates formation of tip cells during angiogenesis. *Nature*. 445: 776–80.

[6] Cohen, M., M. Georgiou, … B. Baum. 2010. Dynamic filopodia transmit intermittent Delta-Notch signaling to drive pattern refinement during lateral inhibition. *Dev. Cell*. 19: 78–89.

[7] Blanco, R., and H. Gerhardt. 2013. VEGF and Notch in tip and stalk cell selection. *Cold Spring Harb. Perspect. Med.* 3: a006569.

[8] Bentley, K., H. Gerhardt, and P. Bates. 2008. Agent-based simulation of notch-mediated tip cell selection in angiogenic sprout initialisation. *J. Theor. Biol.* 250: 25–36.

[9] Carlier, A., L. Geris, …, H. Van Oosterwyck. 2012. MOSAIC: a multiscale model of osteogenesis and sprouting angiogenesis with lateral inhibition of endothelial cells. *PLoS Comput. Biol.* 8: e1002724.

[10] Liu, Z., T. Shirakawa, … A. Soma. 2003. Regulation of Notch1 and Dll4 by vascular endothelial growth factor in arterial endothelial cells: implications for modulating arteriogenesis and angiogenesis. *Mol. Cell. Biol.* 23: 14–25.

[11] Jain, R.K. 2001. Normalizing tumor vasculature with anti-angiogenic therapy: a new paradigm for combination therapy. *Nat. Med.* 7: 987–9.

[12] Lobov, I.B., R.A. Renard, … S.J. Wiegand. 2006. Delta-like ligand 4 (Dll4) is induced by VEGF as a negative regulator of angiogenic sprouting. *Proc. Natl. Acad. Sci.* 4: 1–6.

[13] Risau, W. 1997. Mechanisms of angiogenesis. *Nature*. 386: 671–674.

[14] Metzger, R.J., and M. a Krasnow. 1999. Genetic control of branching morphogenesis. *Science*. 284: 1635–9.

[15] Plate, K., G. Breier, … W. Risau. 1992. Vascular endothelial growth factor is a potential tumour angiogenesis factor in human gliomas *in vivo*. *Nature*. 359: 845–848.

[16] Artavanis-Tsakonas, S. 1999. Notch Signaling: Cell Fate Control and Signal Integration in Development. *Science.* 284: 770–776.

[17] Olsson, A.-K., A. Dimberg, … L. Claesson-Welsh. 2006. VEGF receptor signalling - in control of vascular function. *Nat. Rev. Mol. Cell Biol.* 7: 359–71.

[18] Sawamiphak, S., S. Seidel, … A. Acker-Palmer. 2010. Ephrin-B2 regulates VEGFR2 function in developmental and tumour angiogenesis. *Nature*. 465: 487–91.

[19] Suchting, S., C. Freitas, … A. Eichmann. 2007. The Notch ligand Delta-like 4 negatively regulates endothelial tip cell formation and vessel branching. *Proc. Natl. Acad. Sci. U. S. A.* 104: 3225–30.

[20] Taylor, K.L., A.M. Henderson, and C.C.W. Hughes. 2002. Notch Activation during Endothelial Cell Network Formation *in Vitro* Targets the Basic HLH Transcription Factor HESR-1 and Downregulates VEGFR-2/KDR Expression. *Microvasc. Res.* 64: 372–383.

[21] Holderfield, M.T., A.M. Henderson Anderson, … C.C.W. Hughes. 2006. HESR1/CHF2 suppresses VEGFR2 transcription independent of binding to E-boxes. *Biochem. Biophys. Res. Commun.* 346: 637–48.

[22] Collier, J.R., N. a Monk, … J.H. Lewis. 1996. Pattern formation by lateral inhibition with feedback: a mathematical model of delta-notch intercellular signalling. *J. Theor. Biol.* 183: 429–46.

[23] Caolo, V., N.M.S. van den Akker, … D.G.M. Molin. 2010. Feed-forward signaling by membrane-bound ligand receptor circuit: the case of Notch Delta-like 4 ligand in endothelial cells. *J. Biol. Chem.* 285: 40681–9.

[24] Benedito, R., and M. Hellström. 2013. Notch as a hub for signaling in angiogenesis. *Exp. Cell Res.* 319: 1281–8.

[25] Jakobsson, L., C. a Franco, … H. Gerhardt. 2010. Endothelial cells dynamically compete for the tip cell position during angiogenic sprouting. *Nat. Cell Biol.* 12: 943–53.

[26] Hornig, C., T. Behn, … H. a Weich. 1999. Detection and quantification of complexed and free soluble human vascular endothelial growth factor receptor-1 (sVEGFR-1) by ELISA. *J. Immunol. Methods*. 226: 169–77.

[27] Bentley, K., G. Mariggi, … P. a Bates. 2009. Tipping the balance: robustness of tip cell selection, migration and fusion in angiogenesis. *PLoS Comput. Biol.* 5: e1000549.

[28] Bentley, K., C.A. Franco, … H. Gerhardt. 2014. The role of differential VE-cadherin dynamics in cell rearrangement during angiogenesis. *Nat. Cell Biol.* 16.

[29] Turing, A. 1952. The Chemical Basis of Morphogenesis. *Philos. Trans. R. Soc. London*. 237: 37–72.

[30] Othmer, H.G., and L.E. Scriven. 1971. Instability and Dynamic Pattern in Cellular Networks. *J. Theor. Biol.*

[31] Plahte, E. 2001. Pattern formation in discrete cell lattices. *Math. Biol.* 445: 411–445.

[32] Sprinzak, D., A. Lakhanpal, … M.B. Elowitz. 2010. Cis-interactions between Notch and Delta generate mutually exclusive signalling states. *Nature*. 465: 86–90.

[33] Roukens, M.G., M. Alloul-Ramdhani, … D. a Baker. 2010. Control of endothelial sprouting by a Tel-CtBP complex. *Nat. Cell Biol.* 12: 933–42.

[34] Alon, U. 2007. An Introduction to Systems Biology: Design Principles of Biological Circuits, Vol. 10. Chapman & Hall/CRC, London.

[35] Mac Gabhann, F., and A.S. Popel. 2004. Model of competitive binding of vascular endothelial growth factor and placental growth factor to VEGF receptors on endothelial cells. *Am. J. Physiol. Heart Circ. Physiol.* 286: H153–64.

[36] Waltenberger, J., L. Claesson-Welsh, … C.H. Heldin. 1994. Different signal transduction properties of KDR and Flt1, two receptors for vascular endothelial growth factor. *J. Biol. Chem.* 269: 26988–95.

[37] Wang, D., R.E. Lehman, … M.L. Welton. 2002. Expression and endocytosis of VEGF and its receptors in human colonic vascular endothelial cells. *Am. J. Physiol. Gastrointest. Liver Physiol.* 282: G1088–96.

[38] Takano, S., Y. Yoshii, … T. Nose. 1996. Concentration of Vascular Endothelial Growth Factor in the Serum and Tumor Tissue of Brain Tumor Patients. *Cancer Res.* 56: 2185–2190.

[39] Ilagan, M.X.G., S. Lim, … R. Kopan. 2011. Real-time imaging of notch activation with a luciferase complementation-based reporter. *Sci. Signal.* 4: rs7.

[40] Davis, G.E., K.J. Bayless, and A. Mavila. 2002. Molecular basis of endothelial cell morphogenesis in three-dimensional extracellular matrices. *Anat. Rec.* 268: 252–75.

[41] Cross, V.L., Y. Zheng, … A.D. Stroock. 2010. Dense type I collagen matrices that support cellular remodeling and microfabrication for studies of tumor angiogenesis and vasculogenesis *in vitro*. *Biomaterials*. 31: 8596–607.

[42] Kappas, N.C., G. Zeng, … V.L. Bautch. 2008. The VEGF receptor Flt-1 spatially modulates Flk-1 signaling and blood vessel branching. *J. Cell Biol.* 181: 847–58.

[43] Hashambhoy, Y.L., J.C. Chappell, … F. Mac Gabhann. 2011. Computational modeling of interacting VEGF and soluble VEGF receptor concentration gradients. *Front. Physiol.* 2: 62.

[44] Mac Gabhann, F., and A.S. Popel. 2007. Dimerization of VEGF receptors and implications for signal transduction: a computational study. *Biophys. Chem.* 128: 125–39.

[45] Strogatz, S. 2000. Nonlinear Dynamics and Chaos. Westview Press, USA.

[46] Arima, S., K. Nishiyama, … H. Kurihara. 2011. Angiogenic morphogenesis driven by dynamic and heterogeneous collective endothelial cell movement. *Development*. 138: 4763–76.

[47] Siekmann, A.F., M. Affolter, and H.-G. Belting. 2013. The tip cell concept 10 years after: new players tune in for a common theme. *Exp. Cell Res.* 319: 1255–63.

[48] Seborg, D.E., T.F. Edgar, and D.A. Mellichamp. 1990. Process Dynamics & Control. Wiley, USA.

[49] Shweiki, D., A. Itin, … E. Keshet. 1992. Vascular endothelial growth factor induced by hypoxia may mediate hypoxia-initiated angiogenesis. *Nature*. 359.

[50] Saaristo, A., T. Veikkola, … K. Alitalo. 2002. Adenoviral VEGF-C overexpression induces blood vessel enlargement, tortuosity, and leakiness but no sprouting angiogenesis in the skin or mucous membranes. *FASEB J.* 16: 1041–9.

[51] Albert, R., and H.G. Othmer. 2003. The topology of the regulatory interactions predicts the expression pattern of the segment polarity genes in Drosophila melanogaster. J. Theor. Biol. 223: 1–18.

[52] Barabási, A.-L., and Z.N. Oltvai. 2004. Network biology: understanding the cell's functional organization. *Nat. Rev. Genet.* 5: 101–13.

[53] Owen, M.R., J. a Sherratt, and H.J. Wearing. 2000. Lateral induction by juxtacrine signaling is a new mechanism for pattern formation. Dev. Biol. 217: 54–61.

[54] Nguyen, D.-H.T., S.C. Stapleton, … C.S. Chen. 2013. Biomimetic model to reconstitute angiogenic sprouting morphogenesis *in vitro*. *Proc. Natl. Acad. Sci. U. S. A.* 110: 6712–7.

[55] The Cignal Lenti RBP-Jk Reporter (GFP) Kit is available from SABiosciences, a subsidiary of QIAGEN.

[56] Logsdon, E. a, S.D. Finley, … F. Mac Gabhann. 2013. A systems biology view of blood vessel growth and remodelling. *J. Cell. Mol. Med.* XX: 1–18.

[57] Tompkins, N., N. Li, … S. Fraden. 2014. Testing Turing's theory of morphogenesis in chemical cells. *Proc. Natl. Acad. Sci. U. S. A.* 111: 5753.

[58] Reinitz, J. 2012. Turing centenary: pattern formation. *Nature*. : 2012.